Observations and Modeling of Wave-Acceleration-Induced Sediment Transport in the Surfzone

by

Fernanda Gemael Hoefel

B.S., Fundacao Universidade do Rio Grande, Brazil, 1996
M.S., Universidade Federal do Rio de Janeiro, Brazil, 1998

Submitted in partial fulfillment of the requirements for the degree of

Doctor of Philosophy

at the

MASSACHUSETTS INSTITUTE OF TECHNOLOGY

and the

WOODS HOLE OCEANOGRAPHIC INSTITUTION

February 2004

Author .....
Joint Program in Oceanography/Applied Ocean Science and Engineering
Massachusetts Institute of Technology and
Woods Hole Oceanographic Institution
February, 2004

Certified by .....
Steve Elgar
Thesis Supervisor

Accepted by .....
Dan McCorkle
Chair, Joint Comittee for Marine Geology and Geophysics
Woods Hole Oceanographic Institution

Observations and Modeling of Wave-Acceleration-Induced Sediment Transport in the Surfzone

by

Fernanda Gemael Hoefel

Submitted on February, 2004,
in partial fulfillment of the requirements for the degree of
Doctor of Philosophy

Abstract

Onshore sediment transport and sandbar migration are important to the morphological evolution of beaches, but are not understood well. Here, a new model that accounts for accelerations of wave-orbital velocities predicts onshore sandbar migration observed on an ocean beach. In both the observations and the model, the location of the maximum acceleration-induced transport moves shoreward with the sandbar, resulting in feedback between waves and morphology that drives the bar shoreward until conditions change. A model that combines the effects of transport by waves and mean currents simulates both onshore and offshore bar migration observed over a 45-day period. A stochastic nonlinear Boussinesq model for the evolution of waves in shallow water is coupled with the wave-acceleration-driven sediment transport model to predict observed onshore sediment transport and sandbar migration given observations of the offshore wave field and initial bathymetry. The Boussinesq-wave model has skill in predicting wave spectra, as well as velocity and accceleration statistics across the surfzone, but it underpredicts acceleration skewness on top of the sandbar. As a result, the coupled wave-sediment transport model underpredicts sediment transport, and thus fails to move the sandbar onshore. Although the coupled wave and sediment model can be tuned to yield skillful predictions of onshore sandbar migration, in general, closer agreement between observed and modeled statistics of the wave field is essential for the successful application of wave models to predict sediment transport.

Thesis Supervisor: Steve Elgar

Acknowledgements

First things first. Steve Elgar greatly contributed to every aspect of this thesis (certainly to every sentence). I appreciate very much his generosity, commitment, and invaluable guidance. It has been my privilege to have him as an advisor.

Other people contributed in different but equally important ways. I am grateful to all of them: my thesis committee members, Rob Evans, Edith Gallagher, Ole Madsen, Britt Raubenheimer, and Albert Williams, for the advice, comments, and for all they taught me; Tom Herbers and Mark Orzech for providing the Boussinesq-wave model, and for helping me to understand and implement it; Joe Calantoni, Daniel Conley, Tom Drake, Diane Foster, Bob Guza, Steve Henderson, Tom Herbers, Tom Hsu, Tim Maddux, Pieter Nielsen for all the valuable discussions and comments; the staff of the Academic Programs Office, WHOI, the Joint Committee for Marine Geology and Geophysics (JCMG&G), Susan Humphris and Dan McCorkle for the integral support at all times.

Many thanks to Bob Guza, Tom Herbers, Edith Gallagher, and Britt Raubenheimer for providing the field observations, and also to the staffs of the Center for Coastal Studies, Scripps Institution of Oceanography, and US Army Corps of Engineers Field Research Facility for the excellent logistical support provided during arduous field conditions.

My family and friends (old and new ones) have always made life worthed. It was no different during the last five years, obrigada. For you, meu querido Tom Corbett, I have two words: I do.

Financial support was provided by the Army Research Office (DAAD1999-1-0250 and DAAD19-03-10072); the Office of Naval Research, Coastal Dynamics and Coastal Geosciences Programs (N00014-02-10145); the National Ocean Partnership Program (B-428260); the National Science Foundation, Physical Oceanography (OCE-0115850); and fellowships from Conselho Nacional de Desenvolvimento Cientifico (CNPq) - Brazil (201085/97-6), and from the Academic Programs Office of the Woods Hole Oceanographic Institution.

Contents

List of Figures

Chapter 1

Introduction

Sand bars are ubiquitous morphologic features of sandy beaches. They protect the adjacent beach from direct wave attack and are important expressions of sediment transport patterns in the surfzone, migrating back and forth across the beach responding to and affecting waves and currents, both of which cause sediment transport and morphological evolution, including beach erosion and accretion. Consequently, understanding the processes that cause cross-shore bar migration is necessary to model and predict the behavior of sandy beaches on time scales from days to months.

During high energy wave events, strong offshore directed mean flows (undertow) cause rapid offshore motion of shore-parallel sand bars [Thornton et al., 1996, Gallagher et al., 1998a], whereas during periods of low energy waves, bars move slowly onshore, often becoming crescentic [Wright and Short, 1984, Lippmann and Holman, 1990]. However, the mechanisms responsible for onshore sediment transport and bar migration are not understood, and thus many state-of-the-art models fail to predict the observed beach changes. When bars move onshore undertow is usually weak, and thus oscillatory flows must be the dominant hydrodynamic forcing [Gallagher et al., 1998a, Elgar et al., 2001].

The goal of this thesis is to understand and model the wave-orbital velocity-driven mechanisms responsible for onshore sediment transport and cross-shore sandbar migration in the surfzone. The central hypothesis to be tested is that fluid accelerations associated with pitched-forward waves in the surf zone result in onshore sediment transport

on a natural beach. Nearly continuous observations of waves, near-bottom velocity, and bathymetry collected along a cross-shore transect on a sandy, barred beach near Duck, NC, during the fall of 1994 are used to pursue the following specific objectives:

- Implement and test an acceleration-based sediment transport model that explains onshore sediment transport and bar migration;
- Combine an existing energetics-type cross-shore sediment transport model [Bagnold, 1966, Bowen, 1980, Bailard, 1981], known to have skill in predicting offshore bar migration, with the acceleration-based sediment transport model to reproduce observed patterns of off and onshore sandbar migration during extended periods of time;
- Couple a stochastic Boussinesq wave-shoaling model [Herbers and Burton, 1997, Herbers et al., 2003] with the acceleration-based sediment transport model to reproduce observed onshore bar migration given offshore wave conditions and the initial bathymetry.

1.1 Thesis Outline

The remainder of this chapter presents relevant theoretical background for the accomplishment of the objectives outlined above, followed by a Data and Methods section. Results are introduced in Chapters 2 and 3 in the form of two independent articles. Model calibration is discussed in Appendix A.

Chapter 2, "Wave-Acceleration-Induced Sediment Transport and Sandbar Migration," an extension of Hoefel and Elgar [2003], discusses the effects of wave-acceleration on onshore sediment transport in the surfzone, and the implementation of an acceleration-based sediment transport model that predicts onshore sandbar migration observed on an ocean beach. The model is forced with observed near-bottom fluid accelerations and tested by comparison with observed bathymetric changes. The acceleration-based model is then combined with an energetics sediment transport formulation that reproduces observed sediment transport patterns over a 45-day period during which the sandbar moved offshore during storms, and onshore between storms.

Chapter 3, "Coupled Boussinesq-Wave and Sediment Transport Model Applied to Onshore Sandbar Migration," describes the coupling of a stochastic Boussinesq wave model [Herbers and Burton, 1997, Herbers et al., 2003] to the acceleration-based sediment transport model to predict observed onshore bar migration given observations of the offshore wave field and initial bathymetry.

1.2 Background

The hydrodynamic processes that contribute to cross-shore sediment transport in the nearshore zone include wave-orbital velocities over a range of frequencies, mean currents, and wave breaking-induced turbulence [Bowen, 1980, Bailard, 1981, Roelvink and Stive, 1989, Wright et al., 1991, Thornton et al., 1996, Gallagher et al., 1998a, Ruessink et al., 1998].

During storms, breaking-wave-driven undertow carries suspended sediment offshore [Dally and Dean, 1984, Thornton et al., 1996, Gallagher et al., 1998a]. Cross-shore gradients in undertow, which is maximum just onshore of the bar crest [Thornton et al., 1996, Feddersen et al., 1998, Gallagher et al., 1998a], result in net transport of sediment from onshore to offshore of the bar crest, causing the bar to move offshore. As the bar moves offshore, the locations of wave breaking (on the bar crest) and maximum undertow (onshore of the bar crest) also move offshore, resulting in feedback that promotes continued offshore bar migration as long as there is breaking-induced undertow. Energetics-type sediment transport models [Bowen, 1980, Bailard, 1981], originally developed to describe transport under unidirectional river flow [Bagnold, 1966], accurately predict offshore migration of sandbars observed during storms [Stive, 1986, Russel et al., 1995, Thornton et al., 1996, Gallagher et al., 1998a].

For low energy wave conditions, when the bar is observed to move slowly onshore, wave breaking on the bar and corresponding offshore mean currents are reduced, and sediment transport is predominantly caused by oscillatory flows [Aagaard et al., 1998, Gallagher et al., 1998a]. This transport is usually attributed to the skewed wave orbital velocities associated with the sharp peaks and flat troughs of nonlinear shallow water waves [Bailard, 1981]. In the absence of strong mean flows, a sediment transport formulation

that depends on an odd power of wave-orbital velocity predicts more transport under the larger onshore velocities associated with the sharply peaked wave crests than under the flat, broad, wave troughs, when velocities are offshore. However, velocity-skewness based sediment transport models, such as the energetics model, fail to predict onshore bar migration events observed within the surfzone [Roelvink and Stive, 1989, Russel et al., 1995, Thornton et al., 1996, Gallagher et al., 1998a], mostly owing to the absence of significant cross-shore gradients of velocity skewness near the sand bar.

As waves shoal, their shapes and orbital velocities evolve from skewed profiles in intermediate water depths, to asymmetric, pitched-forward shapes in the surfzone [Elgar and Guza, 1985, Elgar et al., 1988]. The sawtooth-like shape of nearly breaking and broken waves is associated with large fluid accelerations and decelerations during the passage of the steep wave faces, followed by relatively smaller decelerations during the passage of the gently sloping rear of the wave, producing a skewed acceleration profile. Field observations [Hanes and Huntley, 1986, Elgar et al., 2001, Foster et al., 2002], laboratory experiments [Madsen, 1974, Cox et al., 1991, King, 1991, Sleath, 1999], and numerical simulations [Drake and Calantoni, 2001, Hsu and Hanes, in preparation] suggest that fluid accelerations may have a significant effect on sediment transport.

Two-phase sheet flow simulations [Hsu and Hanes, in preparation] corroborate previous field observations [Madsen, 1974, Foster et al., 2002] that indicate severe bed failure under the large flow accelerations, or horizontal pressure gradients, that precede maximum onshore velocities of near-broken waves in the surfzone. If sediment is mobilized by accelerating flows, it is expected that transport will be larger when velocities are onshore directed (just after strong accelerations and decelerations) than during offshore directed flows, resulting in net onshore transport. Discrete-particle computer simulations of sheet flow under unsteady oscillatory flows [Drake and Calantoni, 2001] support this hypothesis and led to the parameterization of acceleration effects of pitched-forward waves in sediment transport as a function of a dimensional form of acceleration skewness (discussed in Chapter 2). Effects of flow acceleration on bedload sediment transport have also been accounted for in a modified, time-varying Shields paramenter [Nielsen, 2002, Nielsen and Callaghan, 2003] used in a Meyer-Peter-type transport formulation to yield sediment

transport predictions.

Observations along a cross-shore transect of the beach near Duck, N.C., extending from the shoreline to 8-m water depth [Elgar et al., 2001], show that acceleration skewness is maximum near the bar crest for a wide range of hydrodynamic conditions and bar crest positions (Figure 1-1). The distribution of cross-shore gradients of acceleration skewness is consistent with erosion offshore (negative gradients) and accretion onshore (positive gradients) of the bar crest (Figure 1-1d). Net onshore sandbar migration would result when mean flows are weak (*e.g.* between days 50 and 60 in Figure 1-1). In contrast, the correlation between bar crest position and location of maximum velocity skewness is low, and cross-shore gradients in velocity skewness could not account for onshore bar migration (not shown, Elgar et al. [2001]).

Energetics Sediment Transport Model

Energetics sediment transport models are among the most used in the surfzone. The original approach was developed by Bagnold [1966] for unidirectional flows, and later it was adapted for oscillatory flows by Bowen [1980] and Bailard [1981]. The model relates sediment transport to fluid power, and it can be written such that it explicitly discriminates between mean-flow, oscillatory-flow, and gravity induced suspended load and bedload. Each term is expressed as a function of odd powers of fluid velocity, sediment characteristics, and efficiency factors that represent the ratio of energy expended in transporting sediment as bedload and suspended load to the total rate of energy production by the stream, given by ϵ_b and ϵ_s, respectively. The total sediment transport rate, Q, is given by [Bagnold, 1966]

$$Q = Q_b + Q_s = \left(\frac{1}{(\rho_s - \rho)g}\right)\left(\frac{\epsilon_b}{\tan\phi - \tan\beta} + \frac{\epsilon_s}{(W/\vec{u}) - \tan\beta}\right) w \qquad (1.1)$$

where subscripts b and s refer to bedload and suspended load, respectively, ρ_s and ρ are the sediment and fluid density, respectively, ϕ is the internal friction angle of the sediment, β is the bed slope, W is the sediment fall velocity, and $\vec{u}$ is the fluid velocity. The last term, w, is the rate of dissipation of energy by the fluid via bed friction and sediment flux.

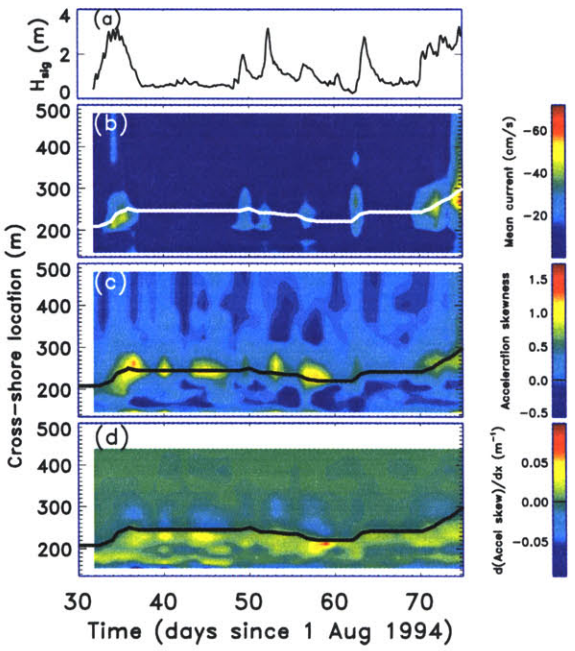

Figure 1-1: Observed wave and near-bottom cross-shore velocity and acceleration statistics from Duck, N.C. (a) Significant wave height of 3-hour long records of sea-surface elevation fluctuations observed in 5-m water depth versus time. Contours of (b) mean current (negative values are offshore-directed), (c) acceleration skewness, and (d) cross-shore gradient of the acceleration skewness as a function of cross-shore location and time. The cross-shore location of the sandbar crest is indicated by the solid curve on each contour plot. In panel d yellow-red contours imply accretion (mostly onshore of the bar crest), and blue-green contours imply erosion (offshore of the bar crest), consistent with onshore motion of sediment, especially when mean currents (panel b) are weak (e.g., between days 50 and 60)(from Elgar et al. [2001]).

For unsteady, oscillatory flows w is a time-varying quantity given by

$$w_{(t)} = \vec{\tau}_{(t)}\vec{u}_{(t)} = \rho C_f |\vec{u}_{(t)}|^3$$

where τ is the bed shear stress, C_f is the drag coefficient, and $\vec{u}_{(t)}$, the velocity vector, consists of u and v components, parallel to the x (cross-shore) and y (alongshore) axes. Following this, the time-averaged, cross-shore volume sediment transport per unit width per unit time is given by [Bowen, 1980, Bailard, 1981]

$$Q_x = K_b\{\langle|\vec{u}|^2\tilde{u}\rangle + \langle|\vec{u}|^2\bar{u}\rangle - \frac{tan\beta}{tan\phi}\langle|\vec{u}|^3\rangle\} + K_s\{\langle|\vec{u}|^3\tilde{u}\rangle + \langle|\vec{u}|^3\bar{u}\rangle - \frac{\epsilon_s}{W}tan\beta\langle|\vec{u}|^5\rangle\} \quad (1.2)$$

where $\bar{u}$ and $\tilde{u}$ are the mean and oscillatory components of the cross-shore near-bottom velocity, respectively, $\tan\beta$ is the local cross-shore beach slope, and angle brackets indicate time average. The coefficients K_b and K_s are

$$K_b = \frac{\rho}{(\rho_s - \rho)g}C_f\frac{\epsilon_b}{\tan\phi}; \qquad K_s = \frac{\rho}{(\rho_s - \rho)g}C_f\frac{\epsilon_s}{W}$$

Bailard [1982] suggested that $\epsilon_b = 0.13$ and $\epsilon_s = 0.01$, similar to the results of Bagnold [1966] for unidirectional flows. Church and Thornton [1993], Thornton et al. [1996], and Gallagher et al. [1998a] have used $\epsilon_b = 0.135$, $\epsilon_s = 0.015$, $C_f = 0.003$, and $\tan\phi = 0.63$.

The cross-shore transport, Q_x (eq. 1.2) is a linear combination of bedload and suspended load, each driven by skewed oscillatory velocities, mean currents, and gravity. The energetics model assumes an instantaneous response of the sediment to the flow and yields a vertically integrated estimate of the transport. Although details of the suspended sediment concentration are not considered, the model uses the ratio between fluid velocity and sediment fall velocity as a surrogate.

1.3 Data and Methods

Pertinent information about observations and data processing techniques are described in Chapters 2 and 3. This section describes general information or details not discussed elsewhere.

Data were collected as part of the Duck94 field experiment conducted on a micro-tidal (*ie*, tidal range < 1 m) ocean beach located near Duck, on the Outer Banks of North Carolina, during the fall of 1994. The beach, roughly oriented north-south, can present one or two sandbars located between 30 and 400 m offshore. The mean foreshore slope of the beach is approximately 4° (1:12) and the mean slope offshore of the bars is approximately 0.3° (1:170) [Lippmann et al., 1993].

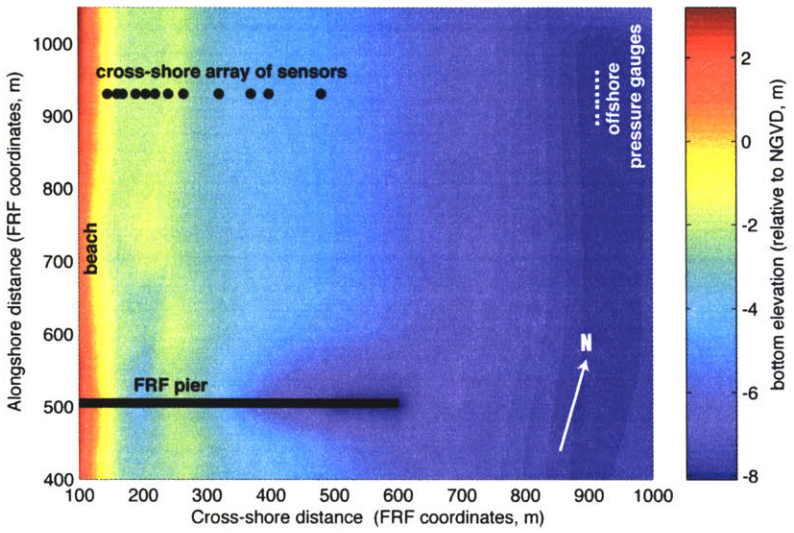

Figure 1-2: Bathymetric map of the field site located near Duck, N.C. Filled black circles represent colocated current meters, pressure gages, and altimeters, filled white squares in 8-m depth represent an array of pressure gages to measure incident waves, and the the Army Corps of Engineers Field Research Facility (FRF) pier is to the south. The map is based on 26 cross-shore bathymetric surveys conducted by the FRF on 20 September 1994. The vertical datum is the National Geodetic Vertical Datum (NGVD).

The data are unique in that they include a wide range of bathymetric and hydrodynamic conditions measured continuously for extended periods of time. Colocated sonar altimeters, pressure sensors, and bidirectional electromagnetic current meters, sampled at 2 Hz, were deployed on fixed frames spanning the inner and outer surfzones, from near the shoreline to approximately 8-m water depth (Figure 1-2). All data were stored in 3-hour-long records. Entire 3-hour records for a particular sensor were discarded if data quality problems were detected, if the sensor was temporarily out of the water owing to tidal fluctuation, or if the sensor was buried or too close to the seafloor due to bathymetric changes. Current meters were adjusted vertically as the bathymetry evolved to maintain an approximately constant elevation of about 50 cm above the seafloor.

Acceleration time series were computed by differentiating measured velocity time series. When applicable, velocity and acceleration time series were Fourier-filtered. Statistical moments, and other averaged quantities, such as sediment transport estimates, were

computed over 3-hour long records. Data gaps were linearly interpolated in time and space.

Based on sediment transport estimates at each sensor location, cross-shore gradients in transport were computed for the mid-points between sensors, and then interpolated back to match sensor locations following Gallagher et al. [1998a].

The seafloor location under each altimeter (averaged over the approximately 6-cm diameter circular footprint of the altimeter) was estimated for every 3-hour period [Gallagher et al., 1996]. Spatially dense surveys were obtained as often as daily using a GPS mounted on the Coastal Amphibious Buggy (CRAB). These surveys were used in conjunction with altimeter measurements to estimate sandbar crest positions.

Surface sediment samples collected along the surveyed beach transect show small temporal variation of cross-shore distribution of grain sizes (not shown) but significant spatial variation, with poorly sorted medium sand in the swash and inner surf zones and well-sorted fine sand seaward (Figure 1-3a). Gallagher et al. [1998a] demonstrated improved energetics model performance by taking into account cross-shore grain size variations. The same procedure is adopted here. Sediment fall velocities were computed according to Jimenez and Madsen [2003] (Figure 1-3b).

Limited observations show significant temporal and spatial cross- and alongshore variations of bedform distribution during the fall of 1994 and 1997 [Thornton et al., 1998, Gallagher et al., 1998b, 2003] that include the occurrence of plane beds, wave-orbital ripples (length scale O(0.1 m),vertical scale O(0.01 m)) , and megaripples (length scale O(1 m), vertical scale O(0.01 m)). For example, under small waves ($H_s < 1$ m) and weak currents (8 Oct 1994) megaripples were observed in the trough and seaward slope of the bar crest, and small ripples were observed on the bar crest, whereas 200 m to the south, in similar water depths, the seafloor displayed a uniform distribution of small ripples, even though the large scale bathymetry was alongshore homogenous [Thornton et al., 1998]. Under moderate storm waves ($H_s \sim 2$ m) and strong alongshore currents (0.5 to 1 m/s), Thornton et al. [1998] observed wave-orbital ripples superimposed on straight-crested megaripples in the inner trough region, lunate megaripples oriented in the direction of the alongshore current on the outer trough, and plane beds seaward of

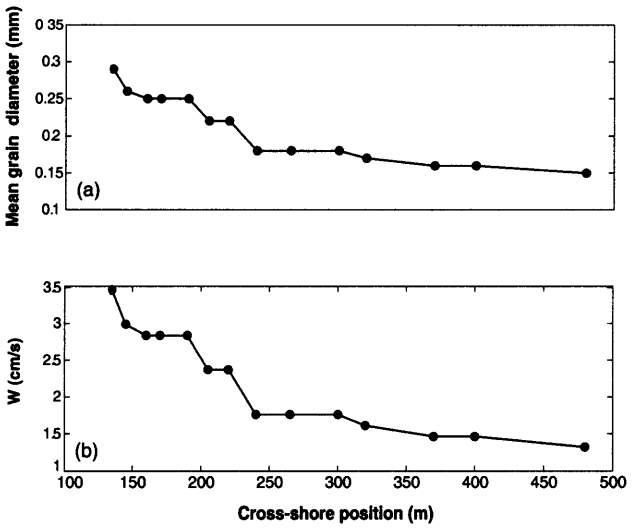

Figure 1-3: (a) Mean grain size and (b) sediment fall velocity, W, versus cross-shore position for samples collected in September 1994.

the bar crest (no observations were made on the bar crest). Following a storm ($H_s \sim 4$ m), megaripples were observed along the axis of a rip current, with plane beds farther alongshore [Thornton et al., 1998].

Correlations of root-mean-square (RMS) bed roughness with mobility number[1] and Shields parameter[2] estimated from measurements over a 500 by 700 m area during the fall of 1997 [Gallagher et al., 2003] suggest the transition from megaripples to plane beds occurs at mobility numbers ~ 150 and Shields parameter ~ 0.5. However, no distinction of regimes can be made below those transitions because the correlation between RMS roughness and mobility number or Shields parameter is poor.

[1]Mobility number: $\psi = \frac{\langle U^2+V^2 \rangle}{(s-1)gD}$, where U and V are the total (wave and current) instantaneous cross- and alongshore velocity components, respectively, s is the specific gravity, D is the mean grain diameter, g is the acceleration of gravity, and angle brackets denote time average.

[2]Shields parameter: $\theta = \frac{\tau}{\rho(s-1)gD}$, where τ is the bed shear stress.

Bibliography

T. Aagaard, J. Nielsen, and B. Greenwood. Suspended sediment transport and nearshore bar formation on a shallow intermediate-state beach. *Marine Geology*, 148:203–225, 1998.

R.A. Bagnold. *An Approach to the Sediment Transport Problem from General Physics.* U.S. Geological Survey, 1966. Professional Paper 422-I.

J.A. Bailard. An energetics total load sediment transport model for a plane sloping beach. *Journal of Geophysical Research*, 86(C11):10938–10954, 1981.

J.A. Bailard. Modeling of on-offshore sediment transport in the surf zone. In *Proceedings of the 18th International Conference in Coastal Engineering*, pages 1419–1438. American Society of Civil Engineering, 1982.

A.J. Bowen. Simple models of nearshore sedimentation of beach profiles and longshore bars. In S.B. McCann, editor, *The Costaline of Canada*, pages 1–11. Geological Survey of Canada Paper 10-80, Ottawa, 1980.

J.C. Church and E.B. Thornton. Effects of breaking wave induced turbulence within a longshore current model. *Coastal Engineering*, 20:1–28, 1993.

D. T. Cox, N. Kobayashi, and H. Mase. Effects of fluid accelerations on sediment transport in surf zones. In *Coastal Sediments' 91*, pages 447–461. ASCE, 1991.

W.R. Dally and R.D. Dean. Suspended sediment transport and beach profile evolution. *Journal of Waterway, Port and Coastal Engineering*, 110:15–33, 1984.

T. G. Drake and J. Calantoni. Discrete particle model for sheet flow sediment transport in the nearshore. *Journal of Geophysical Research*, 106(C9):19859–19868, 2001.

S. Elgar, E. Gallagher, and R.T. Guza. Nearshore sandbar migration. *Journal of Geophysical Research*, 106(C6):11623–11627, 2001.

S. Elgar and R.T. Guza. Observations of bispectra of shoaling surface gravity waves. *Journal of Fluid Mechanics*, 161:425–448, 1985.

S. Elgar, R.T. Guza, and M.H. Freilich. Eulerian measurements of horizontal accelerations in shoaling gravity waves. *Journal of Geophysical Research*, 93(C8):9261–9269, 1988.

F. Feddersen, R.T. Guza, S. Elgar, and T.H.C. Herbers. Alongshore momentum balances in the nearshore. *Journal of Geophysical Research*, 103:15667–15676, 1998.

D.L. Foster, R.A. Holman, and A.J. Bowen. Field evidence for plug flow. *Eos. Transactions AGU*, 83(47), Fall Meeting Suppl., Abstract OS72C-02, 2002.

E. Gallagher, S. Elgar, and R.T. Guza. Observations of sand bar evolution on a natural beach. *Journal of Geophysical Research*, 103(C2):3203–3215, 1998a.

E.L. Gallagher, W. Boyd, S. Elgar, R.T. Guza, and B. Woodsward. Performance of a sonar altimeter in the nearshore. *Marine Geology*, 133:241–248, 1996.

E.L. Gallagher, S. Elgar, and E.B. Thornton. Megaripple migration in a natural surfzone. *Nature*, 394:165–168, 1998b.

E.L. Gallagher, E.B. Thornton, and T.P. Stanton. Sand bed roughness in the nearshore. *Journal of Geophysical Research*, 108(C2):3039, doi:10.1029/2001JC001081 2003.

D.M. Hanes and D.A. Huntley. Continuous measurements of suspended sand concentration in a wave dominated nearshore environment. *Continental Shelf Research*, 6(4):585–596, 1986.

T.H.C. Herbers and M.C. Burton. Nonlinear shoaling of directionally spread waves on a beach. *Journal of Geophysical Research*, 102(C9):21101–21114, 1997.

T.H.C. Herbers, M. Orzech, S. Elgar, and R.T. Guza. Shoaling transformation of wave frequency-directional spectra. *Journal of Geophysical Research*, 108(C1):3013, 2003.

F. Hoefel and S. Elgar. Wave-induced sediment transport and sandbar migration. *Science*, 299:1885–1887, 2003.

T. Hsu and D.M. Hanes. The effects of wave nonlinearity and flow acceleration on coastal sheet flow sediment transport. *Journal of Geophysical Research*, in preparation.

J.A. Jimenez and O.S. Madsen. A simple formula to estimate settling velocity of natural sediments. *Journal of Waterway, Port, Coastal and Ocean Engineering*, 129(2):70–78, 2003.

D. B. King. *Studies in oscillatory flow bed load sediment transport.* PhD thesis, University of California, San Diego, 1991.

T.C. Lippmann and R.A. Holman. The spatial and temporal variability of sand bar morphology. *Journal of Geophysical Research*, 95(C7):11575–11590, 1990.

T.C. Lippmann, R.A. Holman, and K.K. Hathaway. Episodic, nonstationary behavior of a double bar system at Duck, North Carolina, USA. *Journal of Coastal Research*, 15 (SI):49–75, 1993.

O.S. Madsen. Stability of a sand bed under breaking waves. In *Proceedings of the 14th International Conference on Coastal Engineering*, pages 776–794. American Society of Civil Engineering, 1974.

P. Nielsen. Shear stress and sediment transport calculations for swash zone modelling. *Coastal Engineering*, 45:53–60, 2002.

P. Nielsen and D.P. Callaghan. Shear stress and sediment transport calculations for sheet flow under waves. *Coastal Engineering*, 47:347–354, 2003.

J.A. Roelvink and M.J.F. Stive. Bar-generating cross-shore flow mechanics on a beach. *Journal of Geophysical Research*, 94(C4):4185–4800, 1989.

B.G. Ruessink, K.T. Houwman, and P. Hoekstra. The systematic contribution of transporting mechanisms to the cross-shore sediment transport in water depths of 3 to 9 m. *Marine Geology*, 152:295–324, 1998.

P. Russel, Y. Foote, and D. Huntley. An energetics approach to sand transport on beaches. In *Costal Dynamics'95*, pages 829–840, 1995.

J.F.A. Sleath. Conditions for plug flow formation in oscillatory flow. *Continental Shelf Research*, 19:1643–1664, 1999.

M.J.F. Stive. A model for cross-shore sediment transport. In *20th International Conference on Coastal Engineering*, pages 1550–1564. American Society of Civil Engineering, 1986.

E.B. Thornton, R.T. Humiston, and W. Birkemeier. Bar/trough generation on a natural beach. *Journal of Geophysical Research*, 101(C5):12097–12110, 1996.

E.B. Thornton, J.L. Swayne, and J.R. Dingler. Small-scale morphology across the surf zone. *Marine Geology*, 1998:173–196, 1998.

L.D. Wright, J.D. Boon, S.C. Kim, and J.H. List. Modes of cross-shore sediment transport on the shoreface of the Middle Atlantic bight. *Marine Geology*, 96:19–51, 1991.

L.D. Wright and A.D. Short. Morphodynamics variability of surf zones and beaches: A synthesis. *Marine Geology*, 56:93–118, 1984.

Chapter 2

Wave-Acceleration-Induced Sediment Transport and Sandbar Migration

Parts of this chapter were reprinted with permisssion from:
F.Hoefel and S.Elgar, Wave-Induced Sediment Transport and Sandbar Migration,
Science **299**: 1855-1887 (21 Mar 03).

Abstract

Onshore sediment transport and sandbar migration are important to the morphological evolution of beaches, but are not understood well. Here, a model that accounts for fluid accelerations in waves predicts the onshore sandbar migration observed on an ocean beach. In both the observations and the model, the location of the maximum acceleration-induced transport moves shoreward with the sandbar, resulting in feedback between waves and morphology that drives the bar shoreward until conditions change. A model that combines the effects of transport by waves and mean currents simulated both onshore and offshore bar migration observed over a 45-day period.

2.1 Introduction

Surfzone sand bars protect beaches from wave attack, and are a primary expression of cross-shore sediment transport. During storms, intense wave breaking on the bar crest drives strong undertow that carries sediment seaward, resulting in offshore sandbar migration [Thornton et al., 1996, Gallagher et al., 1998a] (Figure 2-1a). If the beach morphology is in equilibrium, the offshore migration is balanced by slower onshore transport between storms [Aubrey, 1979, Wright and Short, 1984]. However, the causes of shoreward sediment transport and sandbar migration are not known, and thus models for beach evolution are not accurate [Roelvink and Stive, 1989, Wright et al., 1991, Thornton et al., 1996, Gallagher et al., 1998a].

As waves enter shallow water, their shapes evolve from sinusoidal to peaky, with sharp wave crests separated by broad, flat wave troughs. It has been hypothesized that the larger onshore velocities under the peaked wave crests transport more sediment than the offshore velocities under the troughs [Bowen, 1980, Bailard, 1981]. However, models that account for the onshore-skewed velocities do not accurately predict onshore bar migration observed near the shoreline and in the surfzone [Roelvink and Stive, 1989, Wright et al., 1991, Thornton et al., 1996, Gallagher et al., 1998a], although skewed velocities may be important outside the surfzone [Trowbridge and Young, 1989]. As waves continue to shoal and break, they evolve from profiles with sharp peaks to asymmetrical, pitched-forward shapes with steep front faces. Water rapidly accelerates under the steep wave front, producing high onshore velocities, followed by smaller decelerations under the gently sloping rear of the wave [Elgar et al., 1988, 2001] (Figure 2-1b). Large accelerations generate strong horizontal pressure gradients that act on the sediment [Madsen, 1974, Drake and Calantoni, 2001, Nielsen, 2002]. Although the precise mechanisms are not fully understood, it has been hypothesized that if accelerations increase the amount of sediment in motion [Hallermeier, 1982, Hanes and Huntley, 1986, Drake and Calantoni, 2001, Elgar et al., 2001], there will be more shoreward than seaward transport under pitched-forward waves.

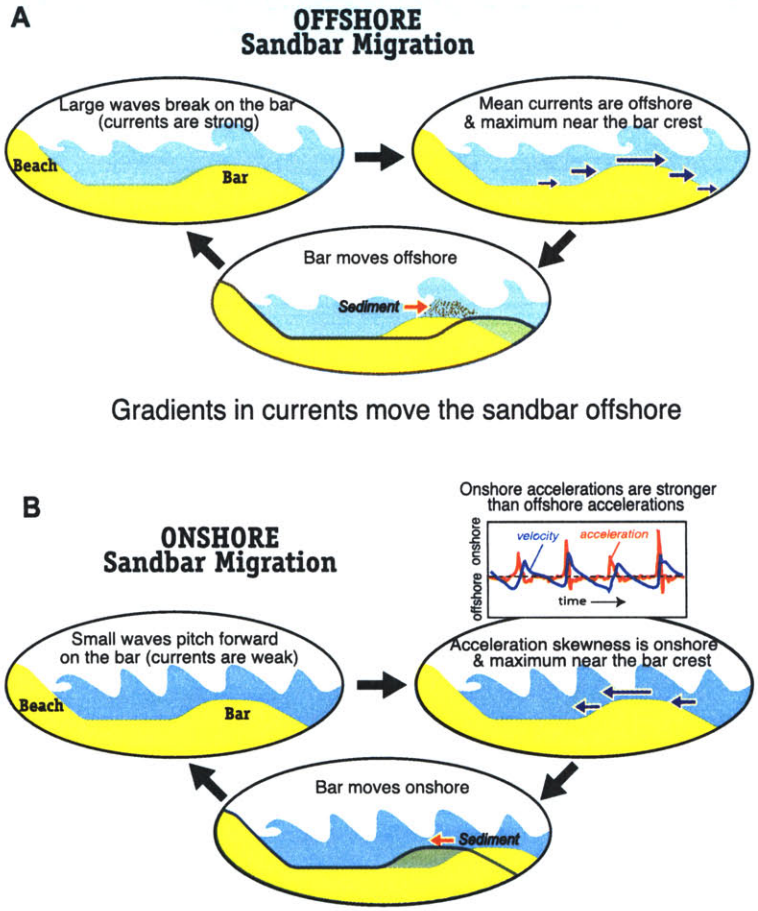

Figure 2-1: Schematic of the feedbacks that drive sandbar migration. (a) Large waves in storms break on the sandbar, driving a strong offshore directed current (undertow) that is maximum just onshore of the bar crest [Gallagher et al., 1998a]. The cross-shore changes (gradients) in the strength of the undertow result in erosion onshore, and deposition offshore of the sandbar crest, and thus offshore bar migration. The location of wave breaking and the maximum of the undertow move offshore with the sandbar, resulting in feedback between waves, currents, and morphological change that drives the bar offshore until conditions change. (b) Small waves do not break on the bar, but develop pitched-forward shapes. Water rapidly is accelerated toward the shore under the steep front face of the waves, and decelerates slowly under the gently sloping rear faces. Thus, the time series of acceleration is skewed, with larger onshore than offshore values (rectangular panel). The cross-shore gradients in acceleration skewness (maximum on the bar crest) result in erosion offshore, and deposition onshore of the bar crest, and thus onshore bar migration. The location of the peak in acceleration skewness moves onshore with the sandbar, resulting in feedback between waves, currents, and morphological change that drives the bar onshore until conditions change.

2.2 Acceleration-based Sediment Transport Model

A surrogate for the effects of acceleration in pitched-forward waves is a dimensional form of acceleration skewness [Drake and Calantoni, 2001] (*ie,* the difference in the magnitudes of accelerations under the front and rear wave faces), $a_{spike} = \langle a^3 \rangle / \langle a^2 \rangle$, where a is the time series of acceleration and angle brackets denote averaging. Discrete-particle computer simulations of bedload transport driven by asymmetrical waves characteristic of surfzones indicate that sediment flux is proportional to a_{spike} once a threshold for sediment motion is exceeded [Drake and Calantoni, 2001]. Unlike the monochromatic waves used in the numerical simulations, accelerations in random waves in a natural surfzone can be skewed either positively (onshore) or negatively (offshore). Thus, the expression for cross-shore (x) acceleration-driven bedload sediment transport $Q_a(x)$ suggested by the numerical simulations is extended to account for random waves by including a term that depends on the sign (*ie*, the direction) of a_{spike}, yielding,

$$Q_a(x) = \begin{cases} k_a(a_{spike} - \text{sgn}[a_{spike}]a_{crit}) & \text{for } |a_{spike}| \geq a_{crit} \\ 0 & \text{for } |a_{spike}| < a_{crit} \end{cases} \tag{2.1}$$

where k_a is a constant, sgn[] is the sign of the argument, and a_{crit} is a threshold that must be exceeded for initiation of transport. By comparing model predictions with observations (see Appendix A for discussion on model calibration), the optimal values of $k_a = 1.40\text{X}10^{-4}$ m s and of $a_{crit} = 0.20$ m s^{-2} were determined. These parameter values are within a factor of 5 of those suggested by the highly idealized discrete particle numerical simulations [Drake and Calantoni, 2001] ($k_a = 0.26\text{X}10^{-4}$ m s, $a_{crit} = 1.00$ m s^{-2}). Differences may be owing to random waves, a distribution of sediment grain sizes and shapes, and breaking-induced turbulence in the ocean. If it is assumed that gradients in alongshore transport are negligible, mass conservation in the cross-shore direction yields

$$\frac{dh}{dt} = \frac{1}{\mu}\frac{dQ_a(x)}{dx} \tag{2.2}$$

where dh/dt is the change in bed elevation h with time t, and $\mu = 0.7$ is a sediment packing

factor. Extensions to Equation 2.2 to account for alongshore changes are straightforward, but not necessary for the small alongshore gradients in transport inferred for the observations discussed here [Gallagher et al., 1998a].

2.3 Results

To test the hypothesis that the cross-shore distribution of near-bottom accelerations result in overall onshore sediment transport and sandbar migration when mean currents are weak, morphological change predicted by the acceleration-based model (Equations 2.1, 2.2) was compared with observations made along a cross-shore transect extending about 400 m from the shoreline to 5-m water depth on the North Carolina coast [Gallagher et al., 1998a]. The model was initialized ($t = 0$) with observed bathymetry and driven with accelerations observed with near-bottom mounted current meters (Figure 2-2). During a 5-day period with approximately 75-cm-high waves and cross-shore mean currents less than 30 cm s^{-1}, the observed onshore sandbar migration of about 30 m was predicted accurately (Figure 2-2). A widely used energetics sediment transport model (Equation 1.2; Bagnold [1966], Bowen [1980], Bailard [1981], Thornton et al. [1996], Gallagher et al. [1998a]) that accounts for transport both by velocity skewness (but not acceleration) and by mean currents predicted no significant changes to the cross-shore depth profile, and thus failed to predict the observed bar migration [Gallagher et al., 1998a] (not shown). Addition of acceleration effects (Equation 2.1) to the energetics sediment transport model results in skilful predictions (Figure 2-2).

During the onshore bar migration event, acceleration skewness (a_{spike}) increased from small values offshore to a maximum near the bar crest, and then decreased toward the shoreline, producing cross-shore gradients in transport that are consistent with erosion offshore and accretion onshore of the bar crest (Figure 2-3). The peak in acceleration skewness moved shoreward with the bar crest (Figure 2-3), resulting in feedback between wave evolution and bathymetry that promoted continued onshore sediment transport and bar movement until conditions changed (Figure 2-1b). Feedback also occurs between wave-breaking induced offshore-directed mean currents (maximum just onshore of the bar

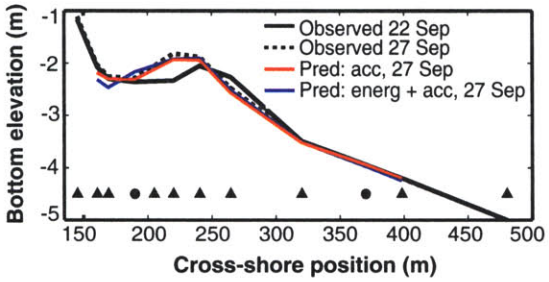

Figure 2-2: Observed and predicted cross-shore bottom elevation profiles. Elevation of the seafloor relative to mean sea level observed 22 Sep 1994 1900 hrs EST (black solid curve), observed 27 Sep 1994 1900 hrs (black dashed curve), and predicted for 27 Sep 1994 1900 hrs by the acceleration-based (red curve) and acceleration plus energetics (using parameters determined previously by Gallagher et al. [1998a], blue curve) sediment transport models versus cross-shore position. Cross-shore locations of colocated pressure sensors, current meters, and altimeters are indicated with triangles, and of colocated pressure sensors and current meters with circles. Observed near-bottom velocities (sampled at 2 Hz) were low-pass filtered (cutoff frequency = 0.5 Hz) and differentiated in time to obtain near-bottom acceleration time series. Sediment transport fluxes for the model predictions were computed from 3-hr averages of observed near-bottom velocity and acceleration statistics, and integrated in time with a 3-hr time step (Equation 2.2) to compute predicted bottom elevation changes. Mean sediment grain sizes ranged from 0.30 mm at the shoreline to 0.15 mm in 5-m water depth (Figure 1-3).

crest) and morphology that results in offshore bar migration during storms [Thornton et al., 1996, Gallagher et al., 1998a] (Figure 2-1a).

During an offshore sandbar migration event observed through a 5-day storm (offshore wave heights > 3 m, and undertow as strong as 60 cm s^{-1} just shoreward of the bar crest), the cross-shore distribution of acceleration skewness also produces transport gradients that drive sediment from offshore to onshore of the bar crest (Figures 1-1 and 2-4). However, during the storm offshore transport by mean flows and skewed velocities, predicted by the energetics model (Equation 1.2), is larger than the acceleration-induced transport (Figure 2-5), resulting in net offshore transport and bar migration that is modeled accurately by the energetics model (Figure 2-6, blue curve). Addition of acceleration-induced transport (Equation 2.1) to the energetics model does not result in significantly different predictions of morphological change during the storm (Figure 2-6, red curve). However, during a 45-day observational period during which the bar crest migrated offshore about 130 m

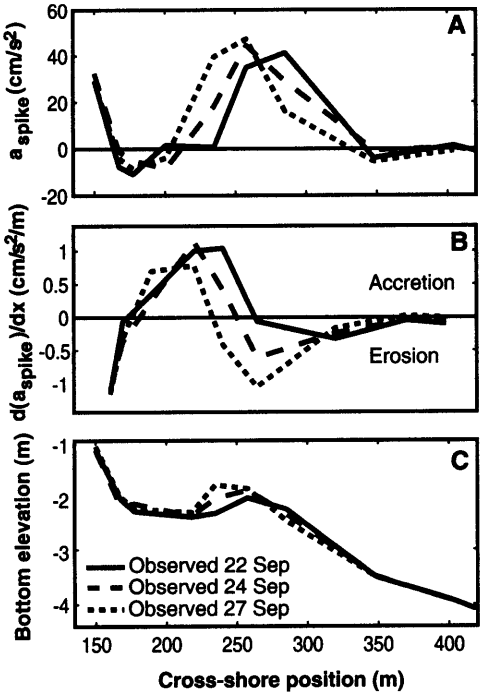

Figure 2-3: Acceleration skewness and bottom elevation profiles during an onshore sandbar migration event. (a) Observed acceleration skewness (a_{spike}), (b) cross-shore gradient of acceleration skewness, and (c) seafloor elevation relative to mean sea level versus cross-shore position. The solid curves are observations from 22 Sep 1900-2200 hrs, dashed curves are 24 Sep 1300-1600 hrs, and dotted curves are 27 Sep 1900-2200 hrs.

during storms and onshore about 40 m when waves and mean flows were small (Figure 2-7a), resulting in a net offshore migration of 90 m, the combined energetics plus acceleration model has significantly higher skill than energetics alone in predicting the evolution of the cross-shore profile. Although the energetics model without acceleration-induced transport predicted the offshore migration, it had limited skill predicting the total change to the beach over 45 days because it failed to predict onshore migration between storms [Gallagher et al., 1998a]. The energetics model extended to include acceleration effects does better predicting the change in the seafloor both onshore and offshore of the bar crest (Figure 2-7), and the overall evolution of the cross-shore bottom elevation profile (Figure 2-8).

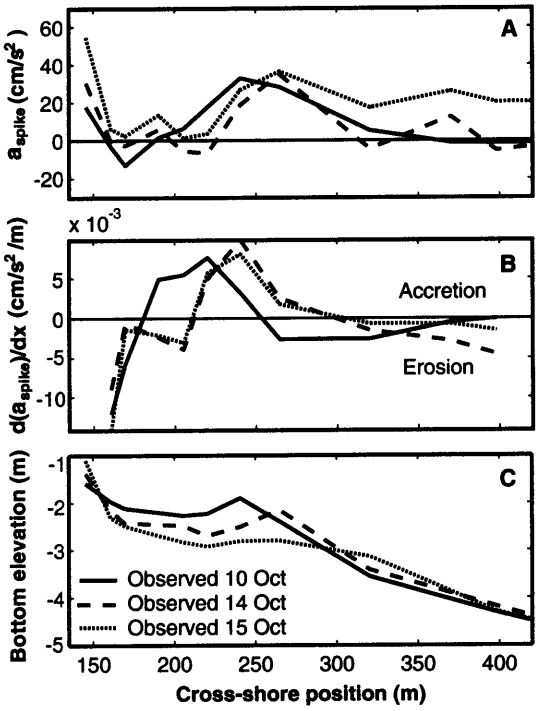

Figure 2-4: Acceleration skewness and bottom elevation profiles during an offshore sandbar migration event. (a) Observed acceleration skewness (a_{spike}), (b) cross-shore gradient of acceleration skewness, and (c) seafloor elevation relative to mean sea level versus cross-shore position. The solid curves are observations from 10 Oct 2200-0100 hrs, dashed curves are 14 Oct 0400-0700 hrs, and dotted curves are 15 Oct 2200-0100 hrs.

2.4 Discussion

The development of sediment transport models has strong empirical character and relies on physical insights and quantitative data obtained in laboratory and field studies [Bowen, 1980, Bailard, 1981, Hallermeier, 1982, Trowbridge and Young, 1989, Dibajnia and Watanabe, 1992, Thornton et al., 1996, Gallagher et al., 1998a, Ribberink, 1998, Dohmen-Janssen, 1999, Malarkey et al., 2003, Nielsen and Callaghan, 2003].

Onshore sediment transport under oscillatory flows has been attributed to skewed (sharp-peaks) near-bottom wave-orbital velocities in the shoaling and surf zones [Bowen, 1980, Bailard, 1981, Dibajnia and Watanabe, 1992, Ribberink, 1998]. Laboratory measurements of transport of fine ($0.15 < D_{50} < 0.20$ mm) sand by second-order Stokes

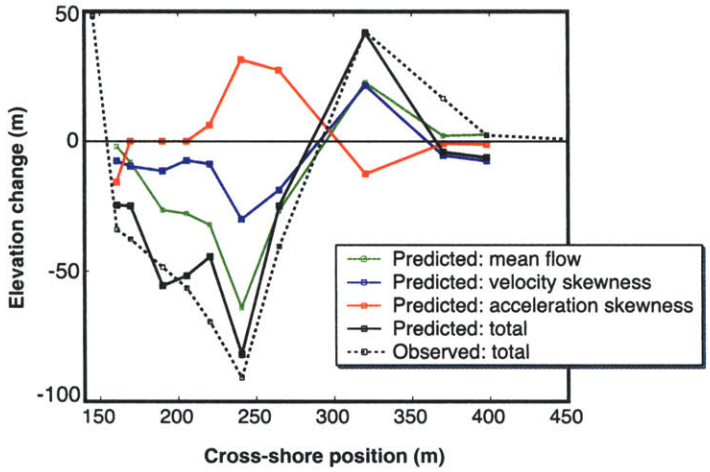

Figure 2-5: Total bottom elevation changes observed and predicted by the combined energetics and acceleration model between 10 Oct 1994, 2200 hours and 15 Oct 1994, 2200 hours versus cross-shore position. Observed bottom elevation changes are shown by the dotted black curve, and changes predicted by individual sediment transport model terms are shown by solid curves: mean-flow-driven changes (green), velocity skewness-driven changes (blue), acceleration skewness-driven changes (red), and total changes (black).

(skewed) waves is consistent with velocity skewness-driven models, which relate sediment transport to an odd power of velocity [Ribberink, 1998, Hassan, 2003], but transport of fine ($D_{50} = 0.24$ mm) and medium ($D_{50} = 0.44$ mm) sand under asymmetrical (pitched-forward) waves is not [King, 1991, Ribberink et al., 2000]. For a perfectly asymmetrical wave (*ie*, no skewness), time averaged odd powers of velocity would be zero, and thus velocity-skewness based transport formulations would predict no transport. Sand transport under pitched-forward waves is modeled more accurately by accounting for fluid accelerations [Nielsen, 1992, 2002]. During the passage of the steep front face of a pitched-forward wave, abrupt accelerations that precede maximum onshore velocities produce thinner boundary layers (*ie*, enhanced bed shear stress) and greater pressure gradients than those produced during the passage of the gently sloping rear face of the wave. A modified shear stress formulation that includes these fluid acceleration effects describes sediment transport in the swashzone [Nielsen, 2002], where waves can have strongly skewed accelerations [Raubenheimer, 2002], and explains bedload transport rates of fine sand ($D_{50} = 0.24$

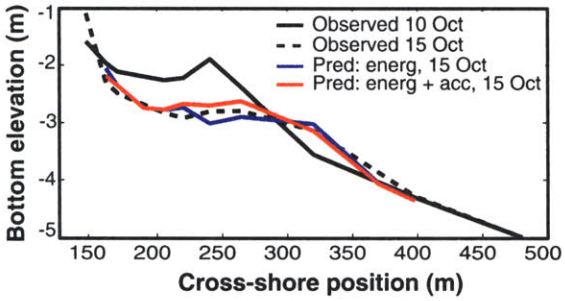

Figure 2-6: Observed and predicted cross-shore bottom elevation profiles. Seafloor elevation relative to mean sea level observed 10 Oct 1994, 2200 hrs (solid black curve), observed 15 Oct 1994, 2200 hrs (dashed black), and predicted for 15 Oct 1994, 2200 hrs by the energetics (blue) and energetics plus acceleration (red) models versus cross-shore position.

mm) observed under pitched-forward laboratory waves [Nielsen and Callaghan, 2003].

In the surfzone, waves are skewed as well as asymmetric [Elgar and Guza, 1985, Elgar, 1987], including during the onshore sandbar migration observed between 22 and 27 September 1994 (Figures 2-2 and 2-9a). However, morphological change requires gradients in sediment transport, and thus depends primarily on the spatial distribution of hydrodynamic forcing. During the onshore sandbar migration event, cross-shore gradients in normalized velocity skewness were small and uncorrelated with sandbar crest position (Figure 2-9b), and therefore were unlikely to have caused net onshore sediment transport and bar migration. In contrast, gradients in normalized acceleration skewness were larger than those in velocity skewness, and imply onshore bar migration (Figure 2-9b).

The precise mechanisms of sediment transport that result in the observed onshore sandbar migration are not understood. Observations by SCUBA divers suggest there was little suspended sediment, and none more than a few cm above the seafloor, consistent with measurements for a range of conditions at this site [Conley and Beach, 2003]. Immediately before the sandbar started to migrate shoreward, the seafloor was smoothed by strong currents (offshore wave height about 2.3 m), and remained relatively smooth for at least a 50-m wide cross-shore section centered on the bar crest during the onshore bar migration (wave heights about 0.75 m) (Figure 2-10). It is hypothesized that bedload dominated sediment transport when the sandbar migrated onshore.

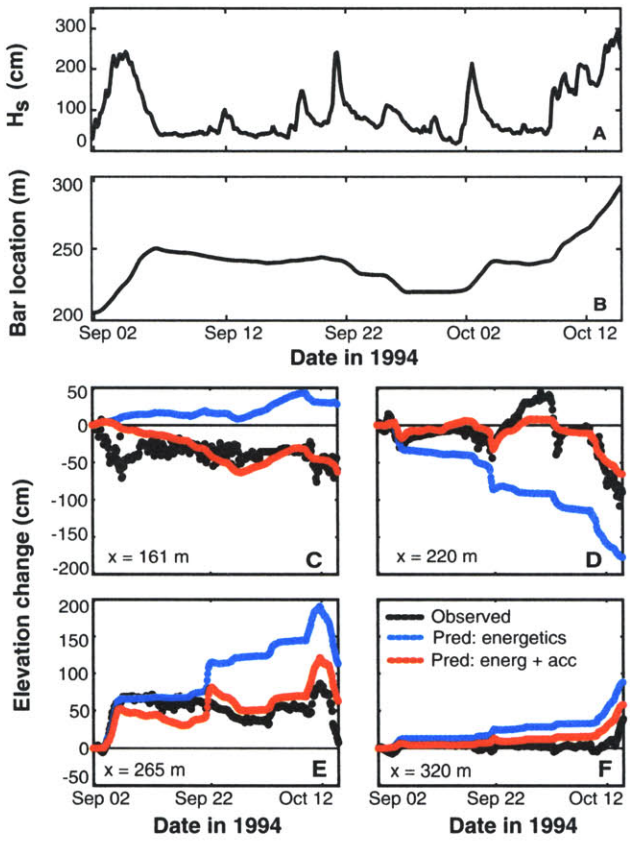

Figure 2-7: Observed wave height, cross-shore sandbar crest position, and observed and predicted bottom elevation changes at four cross-shore locations between 01 Sep 1900 hrs and 15 Oct 2200 hrs. (a) Significant wave height (4 times the standard deviation of 3-hr long records of sea-surface elevation fluctuations in the frequency bands between 0.01 and 0.3 Hz) observed in 5-m water depth and (b) cross-shore position of the sandbar crest versus time. The bar crest position was estimated from spatially dense surveys conducted with an amphibious vehicle approximately bi-weekly, combined with 3-hour-long estimates of seafloor elevation from altimeter measurements [Gallagher et al., 1998a] (Figure 2-2). The shoreline fluctuated (owing to a 1 m tide range) about cross-shore location x=125 m. Observed (black circles) and predicted (blue curve for energetics model, red curve for combined energetics and acceleration model) cumulative change in seafloor elevation at cross-shore locations (c) x=161, (d) x=220, (e) x=265, and (f) x=320 m. Parameters in the energetics model are the same as those in [Gallagher et al., 1998a].

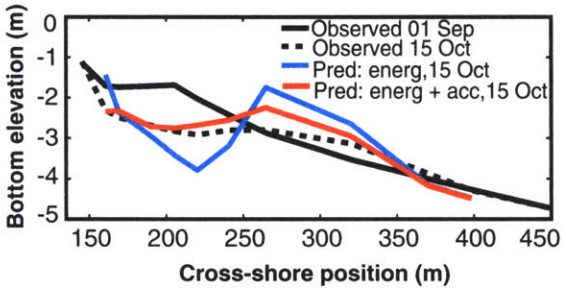

Figure 2-8: Observed and predicted cross-shore bottom elevation profiles spanning a 45-day period. Seafloor elevation relative to mean sea level observed 01 Sep 1900 hrs (solid black curve), observed 15 Oct 2200 hrs (dashed black), and predicted for 15 Oct 2200 hrs by the energetics (blue) and energetics plus acceleration (red) models versus cross-shore position.

Although the details of transport predicted by discrete particle simulations [Drake and Calantoni, 2001] may not be strictly applicable to fine grains transported in a viscous regime, pressure gradients produced by accelerating flows mobilize and move sediment regardless of grain size. Theory [Madsen, 1974], numerical models [Drake and Calantoni, 2001], laboratory measurements [Sleath, 1999], and field observations [Foster et al., 2002] suggest that horizontal pressure gradients can cause a sand bed to become fluidized such that resistance to stress is greatly reduced, thus mobilizing sediment. Sediments in unsteady flows respond to forces associated with flow-induced drag, particle stress (either via collisions for coarse grains or via vicosity of interstitial fluid for concentrated fine grains), and horizontal pressure gradients (caused by accelerating flows). Fine particles respond rapidly (order 0.01 s for 0.2 mm diameter sand) to both drag and particle stresses in concentrated regions. These forces tend to balance each other, potentially allowing slower-acting (order 1 s for ocean waves) horizontal pressure gradient forces to dominate [Hsu and Hanes, in preparation]. In the laboratory [Sleath, 1999] and the field [Foster et al., 2002] blocks or plugs of fine sediment have been observed to move under waves with strong accelerations. Under the pitched-forward waves commonly observed in the surfzone, strong accelerations of near-bottom fluid occur immediately prior to and during onshore-directed wave velocities. Consequently, mobilized sediment will be transported shoreward, consistent with the observations.

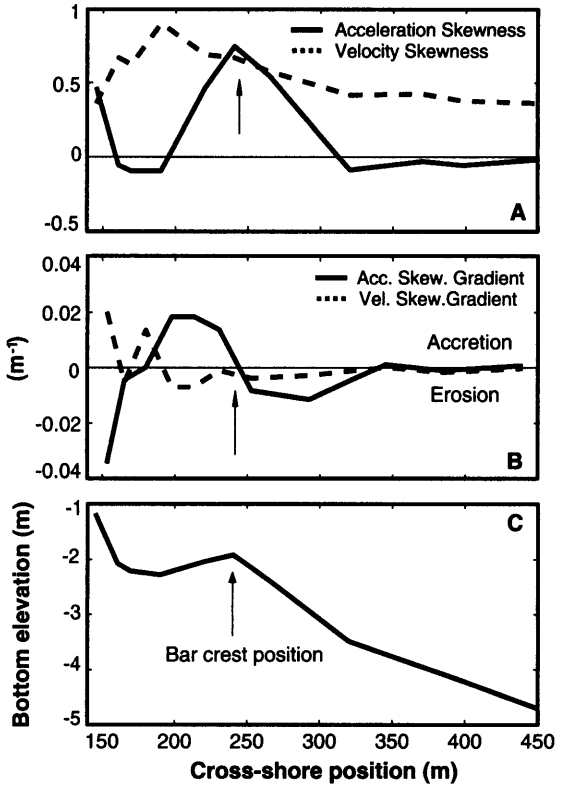

Figure 2-9: Cross-shore distribution of normalized fluid velocity and acceleration skewness (calculated as the mean cube of the demeaned velocity and acceleration time series , respectively, normalized by the variance [Elgar and Guza, 1985]). (a) Near-bottom velocity skewness (dashed curve) and velocity acceleration skewness (solid), (b) cross-shore gradient of velocity (dashed) and acceleration (solid) skewness, and (c) elevation of the seafloor relative to mean seal level versus cross-shore position. Values are averages of observations made between 22 September 1994 1900 hrs EST and 27 September 1994 1900 hrs (*ie*, during the onshore sandbar migration). Positive gradients (panel b) imply accretion and negative gradients imply erosion. The vertical arrows indicate the position of the sandbar crest.

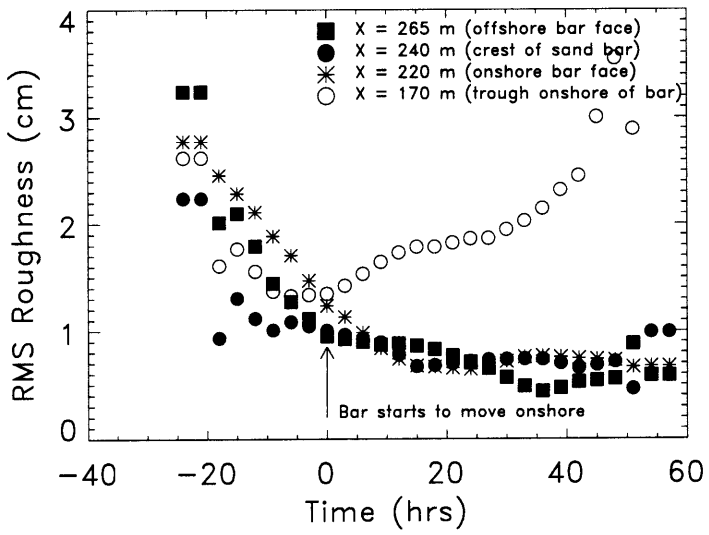

Figure 2-10: Roughness of the seafloor near the sandbar. Root-mean square (rms) seafloor roughness (bedform heights are about 4 times the rms [Gallagher et al., 2003]) versus time before and during the onshore bar migration (time = 0 hrs corresponds to 22 September 1994 1900 hrs EST). Roughness was estimated as the root-mean-square of time series of seafloor location determined by altimeters mounted on fixed frames offshore (squares), on the crest (filled circles), onshore (asterisks), and in the trough (open circles) of the sandbar (the cross-shore positions listed in the legend correspond to those in Figure 2-9). The roughness estimation assumes ripples migrate beneath the altimeters [Gallagher et al., 1998b].

Bibliography

D.G. Aubrey. Seasonal patterns of onshore/offshore sediment movement. *Journal of Geophysical Research*, 84(C10):6347–6354, 1979.

R.A. Bagnold. *An Approach to the Sediment Transport Problem from General Physics.* U.S. Geological Survey, 1966. Professional Paper 422-I.

J.A. Bailard. An energetics total load sediment transport model for a plane sloping beach. *Journal of Geophysical Research*, 86(C11):10938–10954, 1981.

A.J. Bowen. Simple models of nearshore sedimentation of beach profiles and longshore bars. In S.B. McCann, editor, *The Costaline of Canada*, pages 1–11. Geological Survey of Canada Paper 10-80, Ottawa, 1980.

D.C. Conley and R.A. Beach. Cross-shore sediment transport partitioning in the nearshore during a storm event. *Journal of Geophysical Research*, 108(C3):3065, doi:10.1029/2001JC001230, 2003.

M. Dibajnia and A. Watanabe. Sheet flow under nonlinear waves and currents. *Coastal Engineering*, 12:2015–2029, 1992.

M. Dohmen-Janssen. *Grain size influence on sediment transport in oscillatory sheet-flow, phase-lags and modebile-bed effects.* PhD thesis, Delft University of Technology, 1999.

T. G. Drake and J. Calantoni. Discrete particle model for sheet flow sediment transport in the nearshore. *Journal of Geophysical Research*, 106(C9):19859–19868, 2001.

S. Elgar. Relationships involving third moments and bispectra of a harmonic process. *IEEE Transactions on Acoustics, Speech and Signal Processing*, ASSP-35(12):1725–1987, 1987.

S. Elgar, E. Gallagher, and R.T. Guza. Nearshore sandbar migration. *Journal of Geophysical Research*, 106(C6):11623–11627, 2001.

S. Elgar and R.T. Guza. Observations of bispectra of shoaling surface gravity waves. *Journal of Fluid Mechanics*, 161:425–448, 1985.

S. Elgar, R.T. Guza, and M.H. Freilich. Eulerian measurements of horizontal accelerations in shoaling gravity waves. *Journal of Geophysical Research*, 93(C8):9261–9269, 1988.

D.L. Foster, R.A. Holman, and A.J. Bowen. Field evidence for plug flow. *Eos. Transactions AGU*, 83(47), Fall Meeting Suppl., Abstract OS72C-02, 2002.

E. Gallagher, S. Elgar, and R.T. Guza. Observations of sand bar evolution on a natural beach. *Journal of Geophysical Research*, 103(C2):3203–3215, 1998a.

E.L. Gallagher, S. Elgar, and E.B. Thornton. Megaripple migration in a natural surfzone. *Nature*, 394:165–168, 1998b.

E.L. Gallagher, E.B. Thornton, and T.P. Stanton. Sand bed roughness in the nearshore. *Journal of Geophysical Research*, 108(C2):3039, doi:10.1029/2001JC001081 2003.

R.J. Hallermeier. Oscillatory bedload transport: Data review and simple formulation. *Continental Shelf Research*, 1(2):159–190, 1982.

D.M. Hanes and D.A. Huntley. Continuous measurements of suspended sand concentration in a wave dominated nearshore environment. *Continental Shelf Research*, 6(4):585–596, 1986.

W.N.M Hassan. *Transport of size-graded and uniform sediments under oscillatory sheet-flow conditions.* PhD thesis, University of Twente, 2003.

T. Hsu and D.M. Hanes. The effects of wave nonlinearity and flow acceleration on coastal sheet flow sediment transport. *Journal of Geophysical Research*, in preparation.

D. B. King. *Studies in oscillatory flow bed load sediment transport.* PhD thesis, University of California, San Diego, 1991.

O.S. Madsen. Stability of a sand bed under breaking waves. In *Proceedings of the 14th International Conference on Coastal Engineering*, pages 776–794. American Society of Civil Engineering, 1974.

J. Malarkey, A.G. Davies, and Z. Li. A simple model on unsteady sheet-flow sediment transport. *Coastal Engineering*, 48:171–188, 2003.

P. Nielsen. *Coastal Bottom Boundar Layers and Sediment Transport.* World Scientific, 1992.

P. Nielsen. Shear stress and sediment transport calculations for swash zone modelling. *Coastal Engineering*, 45:53–60, 2002.

P. Nielsen and D.P. Callaghan. Shear stress and sediment transport calculations for sheet flow under waves. *Coastal Engineering*, 47:347–354, 2003.

B. Raubenheimer. Observations and predictions of fluid velocities in the surf and swash zones. *Journal of Geophysical Research*, 107(C11):3190–doi:10.1029/2001JC001264, 2002.

J.S. Ribberink. Bed-load transport for steady flows and unsteady oscillatory flows. *Coastal Engineering*, 34:59–82, 1998.

J.S. Ribberink, C.M. Dohmen-Janssen, D. Hanes, S.R. McLean, and C. Vincent. Near-bed sand transport mechanisms under waves: a large scale flume experiment (Sistex99). In *Proceedings of the 27th International Conference on Coastal Engineering*, pages 3263–3276. American Society of Civil Engineers, 2000.

J.A. Roelvink and M.J.F. Stive. Bar-generating cross-shore flow mechanics on a beach. *Journal of Geophysical Research*, 94(C4):4185–4800, 1989.

J.F.A. Sleath. Conditions for plug flow formation in oscillatory flow. *Continental Shelf Research*, 19:1643–1664, 1999.

E.B. Thornton, R.T. Humiston, and W. Birkemeier. Bar/trough generation on a natural beach. *Journal of Geophysical Research*, 101(C5):12097–12110, 1996.

J. Trowbridge and D. Young. Sand transport by unbroken water waves under sheet flow conditions. *Journal of Geophysical Research*, 94(C8):10971–10991, 1989.

L.D. Wright, J.D. Boon, S.C. Kim, and J.H. List. Modes of cross-shore sediment transport on the shoreface of the Middle Atlantic bight. *Marine Geology*, 96:19–51, 1991.

L.D. Wright and A.D. Short. Morphodynamics variability of surf zones and beaches: A synthesis. *Marine Geology*, 56:93–118, 1984.

Chapter 3

Coupled Boussinesq-Wave and Sediment Transport Model Applied to Onshore Sandbar Migration

Abstract

A stochastic Boussinesq model for the nonlinear transformation of surface gravity waves is coupled with a wave-acceleration-driven cross-shore sediment transport model to predict onshore sediment transport and sandbar migration observed on a natural beach. The coupled model is initialized with observed bathymetry and driven with wave frequency-directional spectra estimated from measurements in 8-m water depth. Similar to earlier studies, the wave model has skill in predicting wave frequency spectra, as well as wave velocity skewness and asymmetry across the surfzone. Dimensional acceleration skewness, a third-order moment previously shown to explain onshore sandbar migration in the surf zone, also is predicted fairly well, although modeled values are smaller than observations on the crest of the sandbar. As a result, when driven with modeled acceleration skewness, the sediment transport model (calibrated with observed acceleration moments) underpredicts the rates and cross-shore gradients of sediment transport, failing to move the sandbar onshore. Thus, despite the overall qualitative agreement between observed and modeled statistics of the wave field across the surfzone, closer agreement is essential for the successful application of the Boussinesq-wave model to predict observed sediment transport. Improved skill of the coupled model can be obtained by calibrating the sediment transport model with modeled acceleration moments.

3.1 Introduction

Models for the evolution of ocean surface gravity waves in shallow water are important to the prediction of nearshore circulation and sediment transport. Weakly nonlinear, weakly dispersive Boussinesq wave transformation models accurately predict the observed evolution of sea-surface elevation [Freilich and Guza, 1984, Elgar and Guza 1985b, Elgar et al., 1990, Madsen et al. 1997, Norheim et al., 1998, Herbers et al., 2003, and many others], fluid velocities [Bosboom et al., 1997], and the frequency-directional spectrum [Norheim et al., 1998, Herbers et al., 2003] of waves propagating through the shoaling and surf zones. In addition, Boussinesq models have skill predicting third-order moments (skewness and asymmetry) of velocity [Elgar et al., 1990, Bosboom et al., 1997, Ozanne et al., 2000, Herbers et al., 2003] and velocity acceleration [Elgar et al., 1990] thought to be important to sediment transport [Bowen, 1980, Bailard, 1981, Ribberink, 1998, Drake and Calantoni, 2001, Elgar et al., 2001, Hoefel and Elgar, 2003].

In shallow water ($kh << 1$, where k is the wavenumber magnitude and h is the water depth), nonzero third-order moments of wave-orbital velocity and acceleration arise from near resonant triad nonlinear interactions in which two primary wave components with frequencies f_1 and f_2 and wavenumbers k_1 and k_2 excite a secondary wave component with the sum (f_1+f_2, $k_1+k_2+\delta k$) or difference (f_1-f_2, $k_1-k_2-\delta k$) frequency and wavenumber (where δk is a slight mismatch in the wavenumber), respectively [Freilich and Guza, 1984]. As a result of the energy transfer from the incident wave components to higher and lower frequencies, the wave frequency spectrum is broadened, and the nonlinearly excited secondary wave components are phase-coupled to the primary components, causing deviations of the wave field from Gaussian statistics and the steepening and pitching-forward characteristic of near-breaking waves [Elgar and Guza, 1985a]. Strong accelerations under the steep front of a pitched-forward wave are followed by smaller decelerations under the gently sloping rear of the wave, generating nonzero acceleration skewness that has been used to explain wave-driven onshore sediment transport in the surfzone [Drake and Calantoni, 2001, Hoefel and Elgar, 2003].

Here, a stochastic Boussinesq model for the nonlinear transformation of directionally

spread waves propagating over an alongshore uniform beach [Herbers and Burton, 1997, Herbers et al., 2003] is coupled with a wave-acceleration-skewness-driven sediment transport model [Hoefel and Elgar, 2003] to predict onshore sediment transport and sandbar migration observed on an ocean beach. When driven with observed near-bottom wave-orbital velocities, the sediment transport model predicts the observed onshore sandbar migration [Hoefel and Elgar, 2003]. Although the Boussinesq model qualitatively predicts the evolution of the wave field during the 5-day onshore sandbar migration event, under-prediction of near-bottom fluid acceleration skewness on the sandbar crest results in poor predictions of sediment transport and onshore bar migration. The coupled model predictions are improved by recalibrating model coefficients to account for the discrepancies between observed and modeled acceleration skewness.

3.2 Boussinesq Wave Model

The Boussinesq equations [Peregrine, 1967] are based on assumptions of weak nonlinearity ($a/h << 1$, where a is the wave amplitude) and weak dispersion ($(kh)^2 << 1$) such that the Ursell number, $U = (a/h)/(k/h)^2$, is approximately unity. Stochastic models solve the Boussinesq evolution equations for statistically averaged spectral wave properties, and thus are computationally efficient. However, unlike deterministic models that solve the approximate equations of motion without any assumptions about higher-order statistics, stochastic models require a statistical closure that may yield errors over long propagation distances and in regions of strong nonlinearity [Holloway and Hendershott, 1977]. Thus, a relaxation of the bispectrum to Gaussian statistics over evolution distances comparable with the surfzone width is used in the closure to prevent spurious spatial oscillations and negative spectral values [Orzag, 1970, Herbers and Burton, 1997, Herbers et al., 2003].

Here, a two-dimensional stochastic Boussinesq model for the evolution of the frequency-directional spectrum and bispectrum of surface gravity waves propagating over a gently sloping, alongshore uniform beach [Herbers and Burton, 1997] is used to model the evolution of the wave field across the shoaling and surf zones. Dissipation due to wave breaking is incorporated with a heuristic frequency-dependent term [Kaihatu and Kirby, 1995].

The model, based on a third-order closure (assuming phase coupling between quartets of wave components is weak), is cast in terms of a coupled set of first-order evolution equations for the frequency-alongshore wavenumber (l) spectrum $E(f,l)$ and bispectrum $B(f_1,l_1,f_2,l_2)$. The two-dimensional spectrum $E(f,l)$ defines the energy density of component (f,l), and the four-dimensional (complex) bispectrum $B(f_1,l_1,f_2,l_2)$ defines the average phase relationship of a triad consisting of components (f_1,l_1), (f_2,l_2), and $(-f_1-f_2,-l_1-l_2)$. The integrals of E and B over all frequencies yield, respectively, the mean square and mean cube of the sea-surface elevation. The third-order moments skewness and asymmetry are the integrals of the real and imaginary parts of the bispectrum [Elgar and Guza, 1985a], respectively. Consistent with the depth-averaged Boussinesq equations, linear shallow water transfer functions that neglect vertical variations in the wave-orbital velocity field were used to convert spectra and bispectra of sea-surface elevation to spectra and bispectra of wave-orbital velocity and acceleration, allowing the third-order moments of velocity and acceleration used in the sediment transport model to be estimated from Boussinesq predictions.

Discretized forms of the evolution equations are integrated from the offshore boundary across the beach with a fixed step size of 2 m. The wave model is initialized with bathymetry observed at the beginning of the onshore bar migration event. Offshore boundary conditions are provided by wave frequency-directional spectra $E_0(f,l)$ estimated from 3-hr long records of near-bottom pressure (converted to sea-surface elevation using linear finite depth theory) measured with an array of pressure gages, and the corresponding $B_0(f_1,l_1,f_2,l_2)$ approximated by second-order finite-depth theory (Hasselmann, 1962, Herbers et al., 2003].

The infragravity frequency range $f < 0.05$ Hz was excluded from all bulk wave statistics because strong shoreline reflection of these low-frequency waves is not represented in the model. The maximum wave frequency f_{max} was set to 0.5 Hz to include higher frequency components that may contribute to sediment transport.

3.3 Sediment Transport Model

The importance of wave-acceleration effects on sediment transport has been suggested by field observations [Hanes and Huntley, 1986, Elgar et al., 2001, Foster et al., 2002], laboratory experiments [Madsen, 1974, Cox et al., 1991, King, 1991, Sleath, 1999], and numerical simulations [Drake and Calantoni, 2001, Hsu and Hanes, in preparation]. Although the precise mechanisms involved are not completely understood, two-phase sheet flow simulations [Hsu and Hanes, in preparation] corroborate previous field observations [Foster et al., 2002] that indicate severe bed failure under the large flow accelerations, or horizontal pressure gradients, that precede maximum onshore velocities of pitched-forward nearly-broken or broken waves in shallow water. If sediment is mobilized by accelerating flows, it is expected that transport will be larger when velocities are onshore directed (just after strong accelerations and decelerations) than during offshore directed flows, resulting in net onshore transport. Discrete-particle computer simulations of sheet flow under unsteady oscillatory flows [Drake and Calantoni, 2001] support this hypothesis and led to the parameterization of acceleration effects of pitched-forward waves on sediment transport as a function of a dimensional form of acceleration skewness, $a_{spike} = \langle a^3 \rangle / \langle a^2 \rangle$, where a is the time series of acceleration and angle brackets denote averaging. The expression for cross-shore (x) acceleration-driven bedload sediment transport Q_a suggested by the discrete-particle numerical simulations [Drake and Calantoni, 2001] can be extended to account for random waves in the surfzone, yielding [Hoefel and Elgar, 2003]

$$Q_a(x) = \begin{cases} k_a(a_{spike} - \text{sgn}[a_{spike}]a_{crit}) & \text{for } |a_{spike}| \geq a_{crit} \\ 0 & \text{for } |a_{spike}| < a_{crit} \end{cases} \tag{3.1}$$

where k_a is a constant, sgn[] is the sign of the argument, and a_{crit} is a threshold that must be exceeded for initiation of transport. By comparing model predictions with observations, the optimal values of $k_a = 0.014$ cm s and of $a_{crit} = 20$ cm s^{-2} were determined [Hoefel and Elgar 2003, and also Appendix A]. If it is assumed that gradients in alongshore transport are negligible (as inferred by Gallagher et al. [1998] for the observations discussed here),

mass conservation in the cross-shore direction yields

$$\frac{dh}{dt} = \frac{1}{\mu}\frac{dQ_a(x)}{dx} \tag{3.2}$$

where dh/dt is the change in bed elevation h with time t, and $\mu = 0.7$ is a sediment packing factor.

3.4 Field Observations and Data Analysis

The field observations discussed here were collected on a barrier island beach in the Atlantic Ocean, near Duck, N.C., during an onshore sandbar migration event observed between 22 and 27 September 1994 [Gallagher et al., 1998, Elgar et al., 2001, Hoefel and Elgar, 2003]. Offshore waves were approximately 75-cm high and surfzone cross-shore mean currents were less than 30 cm s^{-1}. Twelve colocated sonar altimeters, pressure sensors, and bidirectional electromagnetic current meters (positioned approximately 50 cm above the seafloor) were mounted on fixed frames deployed from near the shoreline to approximately 5-m water depth [Gallagher et al., 1998, Herbers et al., 2003]. Mean sediment grain sizes along the transect ranged from 0.30 mm at the shoreline to 0.15 mm in 5-m water depth (Figure 1-2, Gallagher et al. [1998]). Beach profiles used to initialize the wave model were obtained through linear interpolation of altimeter measurements. Using high-spatial resolution surveys made with an amphibious vehicle does not change the results presented here.

All instruments were sampled at 2 Hz. Incident wave frequency-directional spectra were estimated from 3-hr long records from a 9-element array of bottom-mounted pressure gauges located in 8-m water depth, about 800 m from the shoreline. Sea-surface elevation frequency-spectra across the transect were estimated from 3-hr-long records of near-bottom pressure using linear finite depth theory. Three-hr long records of observed near-bottom velocities were band-pass filtered (with a Fourier-type filter) between 0.05 and 0.5 Hz to match wave-model output, and differentiated in time to obtain near-bottom acceleration time series. Third-order moments of velocity (skewness and asymmetry) were

calculated as the mean cube of the demeaned time series and Hilbert-transformed time series, respectively, normalized by the variance [Elgar and Guza, 1985a]. Predicted sediment transport fluxes (Equation 3.1) at each sensor location were computed from 3-hr averages of observed or modeled (by the Boussinesq wave model) near-bottom acceleration statistics, and integrated in time with a 3-hr time step (Equation 3.2) to compute predicted bottom elevation changes.

3.5 Coupled Wave and Sediment Transport Model Implementation

The Boussinesq wave model (Section 3.2) was run over the initial observed bathymetry for the first 3-hr boundary condition (22 September 1900 hrs). The results were used to update the bathymetry for the next 3-hr period, the same time interval for which the incident offshore wave spectrum (estimated from observations) was updated, based on sediment transport fluxes (Section 3.3, Equations 3.1 and 3.2) computed from modeled a_{spike} at 8-m intervals along the profile between the offshore pressure-gage array ($x = 800$ m) and the sensor located closest to the shoreline ($x = 145$ m). Tests indicated no significant difference between updating the coupled-model bathymetry at spatial steps of 8 m or at the same locations were sensors were deployed.

The sequence of wave modeling and updating bathymetry every 3 hours was repeated for the 5 day-long onshore migration event. The temporal evolution of the bathymetry, including the relatively slow onshore sandbar migration is well resolved by the 3-hr update cycle.

3.6 Model Application

Previous studies [Elgar et. al, 2001, Hoefel and Elgar, 2003] suggest that onshore sandbar migration can result from feedback between waves and morphology. As waves shoal, velocity acceleration skewness is maximum near the crest of the sandbar, producing cross-shore gradients in acceleration-driven transport that result in erosion offshore, and accretion on-

shore of the bar crest, causing shoreward bar migration. As the sandbar moves shoreward, so does the location of the maximum of acceleration skewness. Thus, accurate predictions of the Boussinesq wave model near the sandbar are of particular importance to modeling morphological evolution. Similar to previous studies [Herbers and Burton, 1997, Herbers et al., 2003], the Boussinesq wave model predicts sea-surface elevation frequency spectra fairly well near the sandbar (Figures 3-1a through 3-1c), except at frequencies above about 0.35 Hz. In all 3 cases, the significant wave height (4 times the standard deviation of sea-surface elevation fluctuations) was about 0.9 m on the bar crest, which was in about 2-m water depth, and thus there was some wave breaking. Deviations between modeled and observed spectral levels at high frequencies may be owing to inaccuracies in the heuristic frequency-dependent dissipation used in the model, or to neglected higher-order nonlinear interactions. The Boussinesq model results shown here (Figures 3-1 through 3-3) are from the coupled wave and sediment transport model, and thus for wave predictions over modeled bathymetry. However, discrepancies between modeled and observed statistics of the wave field likely are not caused by differences between modeled and observed bathymetry because Boussinesq wave statistics over modeled bathymetry are similar to Boussinesq wave statistics over observed bathymetry (not shown).

Even though the cross-shore evolution of velocity skewness (a measure of the difference in shape between wave crests and troughs, with sharp-crested waves having higher skewness) is reproduced qualitatively (Figures 3-1d through 3-1f) by the Boussinesq wave model, predicted values often are higher than observed values, consistent with previous findings (*eg*, Herbers et al. [2003]). Velocity asymmetry (a measure of the difference between the front and rear faces of the waves, with pitched-forward waves having higher asymmetry) is predicted more accurately (Figures 3-1g through 3-1i) than velocity skewness. Velocity asymmetry is closely related to acceleration skewness [Elgar and Guza, 1985a], but less sensitive to high frequency motions [Elgar et al., 1990]. Thus, inaccuracies in Boussinesq model predictions at high frequencies (*eg*, $f > 0.35$ Hz in Figures 3-1a through 3-1c) may have a greater effect on acceleration skewness than on velocity asymmetry (compare Figures 3-1g through 3-1i with Figures 3-2a through 3-2c).

The cross-shore distribution of dimensional acceleration skewness, a_{spike}, is predicted

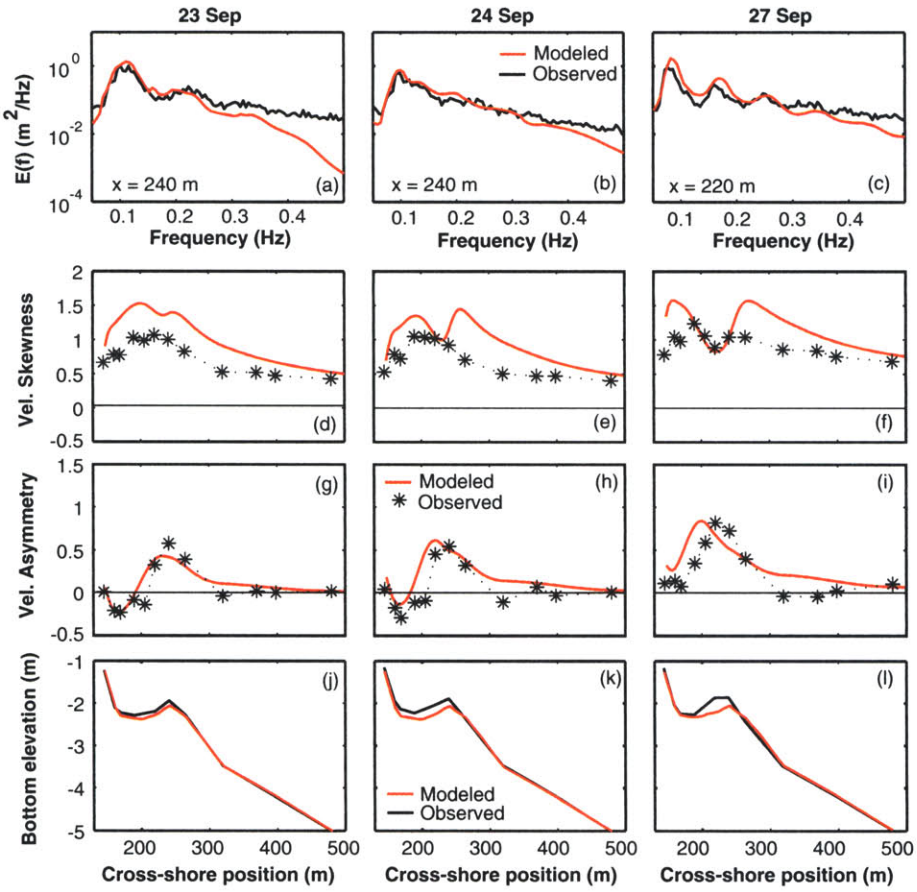

Figure 3-1: Observed (symbols and black curves) and modeled by the coupled Boussinesq wave and acceleration-induced sediment transport model (red curves) sea-surface elevation spectral density near the crest of the sandbar (cross-shore (x) positions are given in each panel) versus frequency for (a) 23 September 1000 hrs, (b) 24 September 1900 hrs, and (c) 27 September 1000 hrs. Spectral estimates have approximately 100 degrees of freedom and 0.0049 Hz frequency resolution. Observed (black symbols) and modeled (red curves) (d-f) near-bottom velocity skewness, (g-i) near bottom velocity asymmetry, and (j-l) seafloor elevation (relative to mean sea level) versus cross-shore position for the same time periods as the corresponding spectra (a-c).

fairly well by the coupled model (Figure 3-2a through 3-2c). For example, on 24 September the agreement between observations and predictions is excellent (Figure 3-2b). However, often a_{spike} is underpredicted on top of the sandbar crest (Figures 3-2a and 3-2c), some-

times falling below the previously determined threshold for acceleration-induced transport, $a_{crit} = 20$ cm s^{-2} (shaded area in Figures 3-2a through 3-2c) [Hoefel and Elgar 2003, and also Appendix A]. As a result, acceleration-induced cross-shore sediment transport (Equation 3.1, with $k_a = 0.014$ cm s and $a_{crit} = 20$ cm s^{-2}) driven by modeled moments also is underpredicted on the sandbar crest compared with transport driven by observed a_{spike} using the same transport model coefficients (Figures 3-2d and 3-2f). Cross-shore gradients of sediment transport estimated from modeled and observed a_{spike} agree qualitatively, and are consistent with erosion offshore (negative gradients), and accretion onshore of the sandbar crest (positive gradients, Figures 3-2g through 3-2i). However, owing to the underprediction of a_{spike} near the sandbar crest, associated sediment transport gradients driven by modeled moments often are smaller than those estimated from observations (*eg*, Figures 3-2g and 3-2i).

During the 5-day onshore sandbar migration event, a_{spike} is underpredicted near the sandbar crest (Figure 3-3a), especially for the highest values of a_{spike}, which are associated with strongly pitched-forward waves, possibly affected by higher-order nonlinear interactions not included in the Boussinesq wave model, and by breaking-induced dissipation that is simulated crudely in the model. Consequently, the coupled model often underpredicts the cross-shore gradients in acceleration-induced sediment transport (Figure 3-3b). Morphological evolution depends on gradients in sediment transport (*eg*, Equation 3.2), so that the underprediction of transport gradients by the coupled model (Figure 3-3b) results in somewhat less erosion offshore, and significantly less accretion onshore of the sandbar crest than is observed and than is predicted by gradients estimated from observed a_{spike} (Figure 3-4). Although the coupled model predicts some of the erosion observed offshore of the sandbar crest ($x = 265$ m, Figure 3-4b), it fails to predict the accretion onshore of the bar crest ($x = 220$ m, Figure 3-4a). As a result, unlike the sediment transport model driven with observed a_{spike}, the coupled model fails to predict the onshore migration of the sandbar (Figure 3-5).

Improved coupled-model skill in predicting observed morphological change would be attained by improving the Boussinesq model predictions, especially near the sandbar crest, perhaps by including higher-order nonlinearities or with a better parameterization of wave

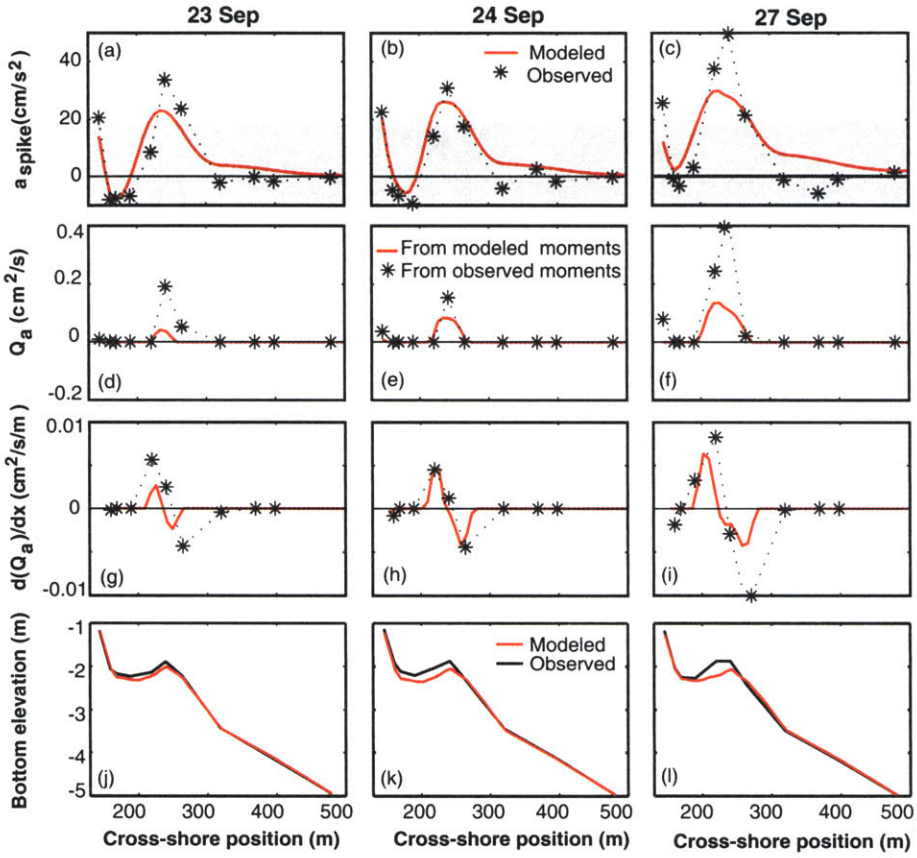

Figure 3-2: (a-c) Observed (symbols and black curves) and modeled (red curves) a_{spike}, associated (d-f) acceleration-induced sediment transport Q_a and (g-i) cross-shore gradients of transport estimated from observed (symbols and black curves) and modeled (red curves) moments, and (j-l) seafloor elevation (relative to mean sea level) versus cross-shore position. Left-hand panels are for 23 September 1000 hrs, middle panels are for 24 September 1900 hrs, and right-hand panels are for 27 September 0100 hrs.

breaking. These improvements are beyond the scope of the present study. Alternatively, the effect of underpredicting a_{spike} on the sandbar crest (*eg*, Figure 3-3a) can be compensated partially by lowering the threshold for initiation of acceleration-induced transport, a_{crit}. Comparison of coupled-model predictions with observations of morphological change suggest that for the onshore migration event discussed here, the highest predictive skill is attained for $a_{crit} = 8$ cm s^{-2} and $k_a = 0.010$ cm s (Figure 3-5).

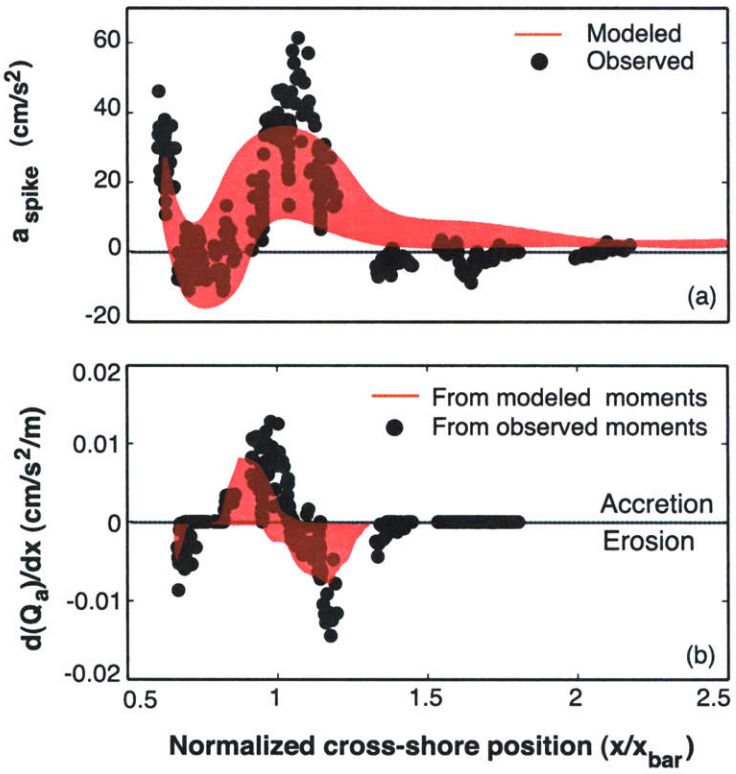

Figure 3-3: (a) Dimensional acceleration skewness (a_{spike}) and (b) cross-shore gradients in acceleration-driven sediment transport Q_a versus cross-shore position (x) normalized by the position of the sandbar crest (x_{bar}). Thus, $x/x_{\text{bar}} = 1$ is the cross-shore position corresponding to the (moving) bar crest. Symbols are observed values, and the red-shaded areas are the envelopes of values predicted by the coupled model from 41 consecutive 3-hr runs beginning 22 September 1900 hrs and ending 27 September 1900 hrs.

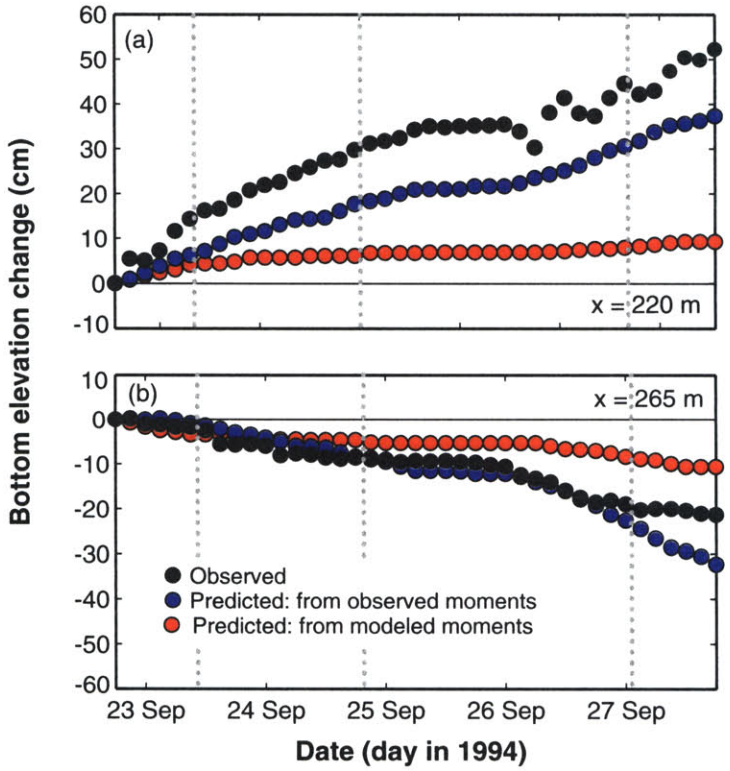

Figure 3-4: Observed (black circles) and predicted (blue circles for sediment transport model driven with observed a_{spike} and red circles for the coupled wave and sediment transport model) cumulative change in seafloor elevation versus time at cross-shore locations (a) x =220 m, and (b) x =265 m. The dotted vertical lines indicate the time periods depicted in Figures 3-1 and 3-2: 23 September 1000 hrs, 24 September 1900 hrs, and 27 September 0100 hrs.

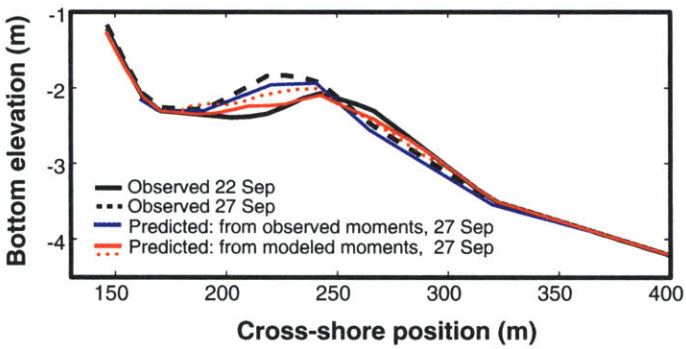

Figure 3-5: Elevation of the seafloor (relative to mean sea level) versus cross-shore position observed on 22 September 1900 hrs (black solid curve), observed on 27 September 1900 hrs (black dashed curve), predicted on 27 September 1900 hrs by the acceleration-based sediment transport model driven with observed a_{spike} (blue solid curve, $a_{crit} = 20$ cm s^{-2}, $k_a = 0.014$ cm s), predicted on 27 September 1900 hrs by the coupled wave and sediment transport model (red solid curve, $a_{crit} = 20$ cm s^{-2}, $k_a = 0.014$ cm s), and predicted on 27 September 1900 hrs by the coupled wave and sediment transport model (red dashed curve, $a_{crit} = 8$ cm s^{-2}, $k_a = 0.010$ cm s).

The sensitivity of the coupled wave and sediment transport model to the choice of high frequency cut-off was briefly investigated. Initially, the same high frequency cut-off (0.5 Hz) used for the data-driven sediment transport model (Chapter 2) was chosen for the Boussinesq wave model. The performance of the sediment transport model driven with observations is insensitive to the choice of high frequency cut-off to the extent that equally skillfull predictions can be obtained for different high frequency cut-offs provided that recalibrated sediment transport model constants are used. However, the underprediction of wave spectral densities by the wave model at frequencies higher than about 0.35 Hz (Figure 3-1a through 3-1c) suggests that the wave model might be sensitive to the choice of high frequency cut-off. Better agreement between observed and modeled moments is obtained by lowering the high frequency cut-off to 0.4 Hz. For this frequency cut-off, both the observation-driven and the coupled Boussinesq-wave sediment transport models yield reasonable agreement with observed profile evolution using the same sediment transport model constants ($a_{crit} = 11$ cm s^{-2}, $k_a = 0.017$ cm s; Figure 3-6).

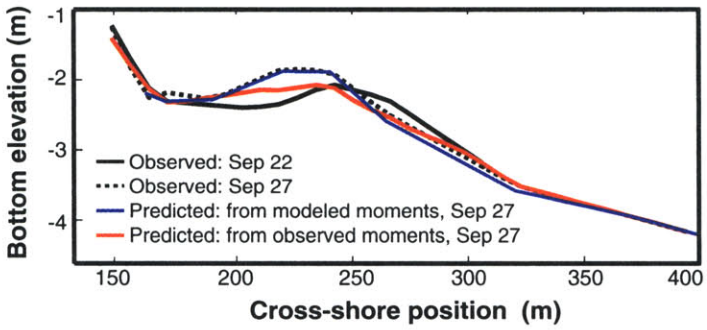

Figure 3-6: Elevation of the seafloor (relative to mean sea level) versus cross-shore position observed on 22 September 1900 hrs (black solid curve), observed on 27 September 1900 hrs (black dashed curve), predicted on 27 September 1900 hrs by the acceleration-based sediment transport model driven with observed a_{spike} (blue solid curve), and predicted on 27 September 1900 hrs by the coupled wave and sediment transport model (red solid curve). For both the data-driven and the coupled wave and sediment transport models the high frequency cut-off was set to 0.4 Hz, and $a_{crit} = 11$ cm s^{-2} and $k_a = 0.017$ cm s.

3.7 Summary

Although the cross-shore evolution of waves shoaling and breaking on a barred beach is modeled well by a stochastic Boussinesq wave model initialized with the wave field observed at the seaward edge of the beach profile [Herbers and Burton, 1997, Herbers et al., 2003], relatively small errors in predicted higher-order moments of the wave field have important effects on subsequent sediment transport and morphological change modeling. In particular, underprediction of near-bottom fluid acceleration skewness near the crest of the sandbar results in reduced skill in acceleration-based sediment transport model predictions relative to predictions based on observed acceleration time series. Consequently, the coupled Boussinesq-wave and acceleration-induced sediment transport model introduced here underpredicts the onshore migration of a sandbar observed on an ocean beach for moderate wave conditions with weak mean cross-shore currents. However, adjustment of model parameters, in particular lowering the threshold for initiation of acceleration-induced sediment transport relative to the optimal threshold determined from data-driven transport modeling, results in improved predictive skill of morphological change. Further research is needed to improve the predictions of the Boussinesq wave model, especially in regions

of strong nonlinearity and wave-breaking induced dissipation (*eg*, near the sandbar crest), and to calibrate sediment transport model coefficients with additional data sets. However, the results presented here suggest that coupling a stochastic Boussinesq wave model with a wave-induced sediment transport model can result in skillful predictions of the onshore sediment transport and sandbar migration observed on an ocean beach when mean currents are weak.

Bibliography

J.A. Bailard. An energetics total load sediment transport model for a plane sloping beach. *Journal of Geophysical Research*, 86(C11):10938–10954, 1981.

J. Bosboom, G. Klopman, J.A. Roelvink, and J.A. Battjes. Boussinesq modelling of wave-induced horizontal particle velocities. *Coastal Engineering*, 32:163–180, 1997.

A.J. Bowen. Simple models of nearshore sedimentation of beach profiles and longshore bars. In S.B. McCann, editor, *The Costaline of Canada*, pages 1–11. Geological Survey of Canada Paper 10-80, Ottawa, 1980.

D. T. Cox, N. Kobayashi, and H. Mase. Effects of fluid accelerations on sediment transport in surf zones. In *Coastal Sediments' 91*, pages 447–461. ASCE, 1991.

T. G. Drake and J. Calantoni. Discrete particle model for sheet flow sediment transport in the nearshore. *Journal of Geophysical Research*, 106(C9):19859–19868, 2001.

S. Elgar and R.T. Guza. Observations of bispectra of shoaling surface gravity waves. *Journal of Fluid Mechanics*, 161:425–448, 1985a.

S. Elgar and R.T. Guza. Shoaling gravity waves: Comparisons between field observations, linear theory, and a nonlinear model. *Journal of Fluid Mechanics*, 158:47–70, 1985b.

S. Elgar, M.H. Freilich, and R.T. Guza. Model-data comparisons of moments of non-breaking shoaling surface gravity waves. *Journal of Geophysical Research*, 95(C9): 16055–16063, 1990.

S. Elgar, E. Gallagher, and R.T. Guza. Nearshore sandbar migration. *Journal of Geophysical Research*, 106(C6):11623–11627, 2001.

D.L. Foster, R.A. Holman, and A.J. Bowen. Field evidence for plug flow. *Eos. Transactions AGU*, 83(47), Fall Meeting Suppl., Abstract OS72C-02, 2002.

M.H. Freilich and R.T. Guza. Nonlinear effects on shoaling surface gravity waves. *Philosophical Transanctions of the Royal Society of London*, A311:1–41, 1984.

E. Gallagher, S. Elgar, and R.T. Guza. Observations of sand bar evolution on a natural beach. *Journal of Geophysical Research*, 103(C2):3203–3215, 1998.

D.M. Hanes and D.A. Huntley. Continuous measurements of suspended sand concentration in a wave dominated nearshore environment. *Continental Shelf Research*, 6(4):585–596, 1986.

T.H.C. Herbers and M.C. Burton. Nonlinear shoaling of directionally spread waves on a beach. *Journal of Geophysical Research*, 102(C9):21101–21114, 1997.

T.H.C. Herbers, M. Orzech, S. Elgar, and R.T. Guza. Shoaling transformation of wave frequency-directional spectra. *Journal of Geophysical Research*, 108(C1):3013, 2003.

F. Hoefel and S. Elgar. Wave-induced sediment transport and sandbar migration. *Science*, 299:1885–1887, 2003.

G. Holloway and M.C. Hendershott. Stochastic closure for nonlinear Rosby waves. *Journal of Fluid Mechanics*, 82:747–765, 1977.

T. Hsu and D.M. Hanes. The effects of wave nonlinearity and flow acceleration on coastal sheet flow sediment transport. *Journal of Geophysical Research*, in preparation.

J.M. Kaihatu and J.T. Kirby. Nonlinear transformation of waves in finite water depth. *Physics of Fluids*, 7:1903–1914, 1995.

D. B. King. *Studies in oscillatory flow bed load sediment transport.* PhD thesis, University of California, San Diego, 1991.

O.S. Madsen. Stability of a sand bed under breaking waves. In *Proceedings of the 14th International Conference on Coastal Engineering*, pages 776–794. American Society of Civil Engineering, 1974.

P.A. Madsen, O.R. Sorensen, and H.A. Shaffer. Surf zone dynamics simulated by a Boussinesq type model: Part I model description and cross-shore motion of regular waves. *Coastal Engineering*, 41:361–397, 1997.

C.A. Norheim, T.H.C. Herbers, and S. Elgar. Nonlinear evolution of surface wave spectra on a beach. *Journal of Physical Oceanography*, 28:1534–1551, 1998.

S.A. Orzag. Analytical theories of turbulence. *Journal of Fluid Mechanics*, 41:363–386, 1970.

F. Ozanne, A. Chadwick, D.A. Huntley, D.A. Simmonds, and J. Lawrence. Velocity predictions for shoaling and breaking waves with a Boussinesq-type model. *Costal Engineering*, 41:361–397, 2000.

D.H. Peregrine. Long waves on a beach. *Journal of Fluid Mechanics*, 27:815–827, 1967.

J.S. Ribberink. Bed-load transport for steady flows and unsteady oscillatory flows. *Coastal Engineering*, 34:59–82, 1998.

J.F.A. Sleath. Conditions for plug flow formation in oscillatory flow. *Continental Shelf Research*, 19:1643–1664, 1999.

Appendix A

Combined Energetics and Acceleration Model Performance

Model performance can be quantified by means of the normalized root mean square (RMS) prediction error E_{RMS}/Δ_{RMS}, where E_{RMS} is the RMS error between final predicted and observed 3-hour averaged profiles and Δ_{RMS} is the RMS change between the initial and final observed profiles. Model skill is defined as (after Davis [1976] and Gallagher et al. [1998])

$$skill = 1 - \frac{E_{RMS}}{\Delta_{RMS}} \tag{A.1}$$

where,

$$E_{RMS} = \sqrt{\frac{1}{N}\sum_{n=1}^{N}\left[S_n(h_{predicted,n} - h_{observed,n})\right]^2} \tag{A.2}$$

and

$$\Delta_{RMS} = \sqrt{\frac{1}{N}\sum_{n=1}^{N}\left[S_n\Delta_n\right]^2} \tag{A.3}$$

where N is the number of sensors along the cross-shore transect, $h_{predicted,n}$ is the predicted

final profile at each location n, $h_{observed,n}$ is the observed final profile, and Δ_n is the measured change in seafloor elevation at each of the N sensor locations. To account for irregular sensor spacing, estimates at each cross-shore location are weighted by S_n given by

$$S_n = \begin{cases} \frac{\frac{1}{2}(dx_{n-1}+dx_n)}{\overline{dx}} & \text{for } n = 2, ..., N-1 \\ \frac{dx_n}{\overline{dx}} & \text{for } n = 1, N \end{cases} \tag{A.4}$$

where $dx_n = x_{n+1} - x_n$ is the separation between adjacent sensors located at cross-shore positions x_{n+1} and x_n, and $\overline{dx}$ is the average sensor separation along a transect.

Model skill is maximum and equal to 1 when there is perfect agreement between final observed and predicted profiles. If $skill = 0$, prediction errors are as large as observed changes, whereas if $skill < 0$ prediction errors are larger than observed changes. If observed changes between initial and final profiles are small (*ie*, Δ_{RMS} is small), the corresponding model skill may be low even if errors (E_{RMS}) in predictions are small [Gallagher et al., 1998].

The skill of the combined acceleration and energetics model was evaluated as a function of the acceleration-based model constants k_a and a_{crit} for three simulation periods for the Duck94 data set (Figure A-1). These periods include the onshore bar migration event between 22 and 27 Sep (Figure 2-2), an offshore bar migration event observed during a storm between 10 Oct and 15 Oct (Figure 2-6), and a 45-day long simulation between 01 Sep and 15 Oct that includes on and offshore bar migration events, as well as lower energy wave events during which no significant bathymetric changes were observed (Figure 2-7). Calibration and model performance of the energetics formulation has been evaluated previously by Thornton et al. [1996], and Gallagher et al. [1998].

Simulations for the onshore bar migration event (22 to 27 Sep, Figure A-1a) indicate little model sensitivity to k_a (*ie*, the maximum skill of approximately 0.7 is attained for $0.02 < k_a < 0.2$ cm s) and large sensitivity to the acceleration threshold for sediment transport, a_{crit} (*ie*, maximum model skill is attained for a narrow range of a_{crit}). A similar sensitivity to k_a and a_{crit} is observed for the offshore bar migration event (10 to 15 Oct, Figure A-1b). Including the effects of acceleration-induced transport (*ie*, when $a_{crit} < 50$

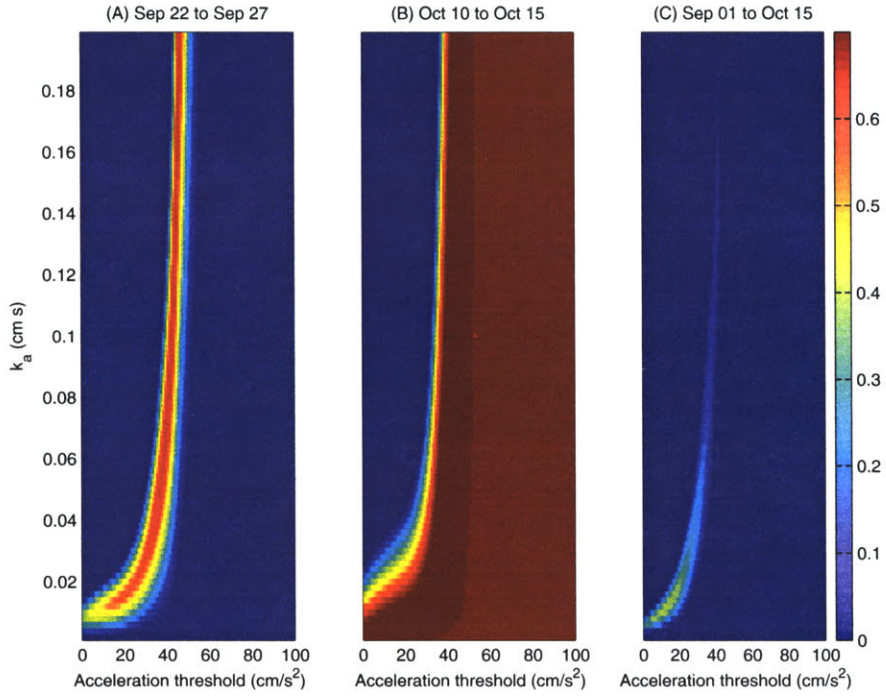

Figure A-1: Combined energetics and acceleration sediment transport model skill as a function of k_a and a_{crit} for three simulations. (a) 22 Sep to 27 Sep, 1994 (onshore bar migration event); (b)10 Oct to 15 Oct, 1994 (offshore bar migration event); and (c) Sep 01 to Oct 15 (onshore and offshore bar migration events). All skills ≤ 0 were grouped into the $skill = 0$ bin for better visualization.

cm/s^2) results in improved skill relative to predictions of the energetics model alone (*ie*, when $a_{crit} > 50$ cm/s^2). Simulations that include on and offshore bar migration events, as well as periods with no significant bathymetric changes, indicate a limited optimum parameter space centered around the values of $k_a \sim 0.01$ cm s and $a_{crit} \sim 20$ cm/s^2 (Figure A-1c).

Bibliography

R.E. Davis. Predictability of sea surface temperature and sea level pressure anomalies over the North Pacific ocean. *Journal of Physical Oceanography*, 6:249–266, 1976.

E. Gallagher, S. Elgar, and R.T. Guza. Observations of sand bar evolution on a natural beach. *Journal of Geophysical Research*, 103(C2):3203–3215, 1998.

E.B. Thornton, R.T. Humiston, and W. Birkemeier. Bar/trough generation on a natural beach. *Journal of Geophysical Research*, 101(C5):12097–12110, 1996.